Interleukin enhancer binding factor 2 (Ilf2) and kidney epithelial stress resilience

Shuang Cao (M.Sc.) [1,2,3], Karen I. López-Cayuqueo (PhD) [1], Janna Leiz [2,3], Felix J. Boivin [2,3], Lajos Markó (MD, PhD) [3], Christian Hinze (MD) [1], Kai M. Schmidt-Ott (MD) [1,2,3,*]

[1] Department of Nephrology and Hypertension, Hannover Medical School (MHH), Hannover, Germany.

[2] Department of Nephrology and Medical Intensive Care, Charite´ - Universitätsmedizin Berlin, Corporate Member of Freie Universität Berlin and Humboldt-Universität zu Berlin, Berlin, Germany

[3] Experimental and Clinical Research Center, a cooperation between the Charité Medical Faculty and the Max-Delbrück Center for Molecular Medicine, Berlin, Germany

[*]**Corresponding author:** Prof. Dr. med. Kai Schmidt-Ott, Department of Nephrology and Hypertension, Hannover Medical School (MHH), 30625 Hannover, Germany.

Tel: +495115326320

Fax: +49511552366

Email: Schmidt-Ott.Kai@mh-hannover.de

Abstract

Introduction

In the kidney, epithelial cells of medullary collecting ducts (MCD) are exposed to a harsh microenvironment characterized by hyperosmolality, hypoxia, and oxidative stress. Still, under physiological conditions, they show no apparent signs of cellular injury. We hypothesized that the study of transcription factors (TFs) enriched in MCD cells might identify pathways of stress resilience.

Methods

We generated single-cell expression data from mouse kidneys and predicted *in silico* candidate TFs with MCD-enriched expression and activity. To investigate the transcriptomic effects of perturbing these candidate TFs, we devised a single-cell CRISPR interference (CRISPRi) screen in mouse inner medullary collecting duct (IMCD3) cells.

Results

We found that perturbation of interleukin enhancer-binding factor 2 (Ilf2), Krueppel-like factor 5 (Klf5), and JunB proto-oncogene (Junb), significantly impacted IMCD3 cells' gene expression programs, including genes involved in proliferation, apoptosis, and stress-related intracellular signaling, highlighting these TFs as potential regulators of cell-specific resilience. We then focused on Ilf2, validated its impact on gene expression signatures by RNA sequencing, and identified a further role of Ilf2 in the splicing of genes involved in epithelial cellular dynamics and stress responses. Loss of Ilf2 function in IMCD3 cells resulted in nuclear atypia, reduced proliferative

capacity, and increased cell death in response to osmotic stress. Ilf2 was upregulated in mouse kidneys during the repair phase following ischemia-reperfusion injury (IRI), as were Ilf2-regulated transcripts and splicing events, suggesting that Ilf2 might serve as a post-ischemic signal to facilitate epithelial stress resilience.

Conclusions

Our approach nominates novel pathways of cellular resilience in kidney tubular cells and highlights Ilf2 as a potential target for kidney protection.

Keywords

kidney medullary epithelial cells; stress resilience; nuclear integrity; RNA splicing; proliferation; repair.

Translational Statement

We identify Ilf2 as a transcriptional regulator promoting the stress resilience of renal epithelial cells. Our study provides mechanistic insights into the endogenous mechanisms that protect kidney epithelia from the adverse microenvironment of the renal medulla. Furthermore, Ilf2 activation might constitute a broader mechanism to preserve kidney epithelial integrity under injurious conditions.

Introduction

The mammalian kidney plays a central role in fluid and electrolyte homeostasis, clearance of metabolic waste products, and conservation of free water. These functions depend on a complex cortico-medullary organization of the organ. Urine concentration is driven by the countercurrent multiplier and urea recycling systems, which establish high sodium and urea levels and thus hyperosmolarity in the renal

medullary interstitium. This osmotic gradient facilitates transcellular water reabsorption from the collecting duct lumen.

The accumulation of sodium, chloride, and urea in the medullary interstitium imposes osmotic stress on medullary collecting duct cells[1]. Furthermore, the medulla operates under relative hypoxia due to limited blood flow and relatively high metabolic activity, leading to elevated levels of reactive oxygen species (ROS)[2,3]. Despite these harsh conditions, collecting duct epithelial cells not only survive but also actively adapt to environmental fluctuations[4].

During acute kidney injury (AKI), tubular stress resilience becomes particularly critical in response to ischemia, hypoxia, or nephrotoxins[5]. Under such stressors, cells within the tubular system exhibit heterogeneous susceptibility to damage. Risk factors such as aging, preexisting kidney disease and comorbidities further heighten vulnerability to injury. Importantly, this heterogeneity extends to different tubular cell types. For example, collecting duct cells are notably more resistant to injury than proximal tubule cells[6]. This observation raises the question: what specific mechanisms confer resilience to stress in collecting duct cells?

TFs play a central role in orchestrating gene expression programs that mediate cellular responses to environmental stress and adaptation[7–9]. In collecting duct principal cells, TFs such as Grainyhead-like 2 (GRHL2) and Nuclear Factor of Activated T-Cells 5 (NFAT5) regulate epithelial integrity and osmotic homeostasis. GRHL2 maintains tight junction function and prevents solute leakage[10], while NFAT5 activates osmoprotective genes such as aquaporin-2 (AQP2) in response to hypertonic stress[11,12]. Dysregulation of these pathways is implicated in conditions such as hypertension, chronic kidney disease, and electrolyte disturbances[13,14],

underscoring the importance of understanding their transcriptional control. Although several osmoprotective mechanisms have been described in renal medullary cells[12,15–17], the transcriptional programs underlying stress resilience in medullary collecting duct cells remain poorly defined.

Despite advances in single-cell transcriptomics and computational tools, functional validation of candidate TFs remains a significant challenge. Traditional approaches, such as single-gene knockouts, are time-consuming, costly, and lack scalability, making it difficult to assess gene function across a large number of candidate regulators. To address these limitations, single-cell CRISPR screening has emerged as a powerful approach for dissecting gene regulatory networks at high resolution. By integrating CRISPR interference (CRISPRi) with single-cell RNA sequencing (scRNA-seq), this strategy enables the functional interrogation of multiple genes of interest within a single experiment[18,19]. CRISPRi employs a catalytically inactive Cas9 (dCas9) fused to a transcriptional repressor, guided by single guide RNA (sgRNA), to selectively repress expression of any gene of interest without altering the genome. The scRNA-seq readouts allow for simultaneous capture of sgRNA identity and downstream transcriptomic effects across diverse cell populations[20]. This method is suited for investigating how TFs coordinate gene expression programs.

In this study, we sought to identify the molecular pathways underlying stress resistance in medullary collecting duct cells. We first used computational prediction based on single-nucleus RNA sequencing data from mouse kidneys to nominate candidate TFs that are enriched and transcriptionally active in medullary collecting ducts. We then applied CRISPRi combined with scRNA-seq to systematically silence these candidate TFs and assess resulting transcriptomic changes. Our study

identified and validated Ilf2 as a regulator of stress resilience in kidney epithelial cells - a discovery with potential translational significance.

Methods

Detailed methods used in this study were provided in the Supplementary Materials.

Animals

All animal procedures were approved by local authorities (LAGeSo, Berlin) and conducted on 8- to 12-week-old male mice under standard housing conditions at the MDC animal facility.

snRNA-seq Data Processing and Analysis

Data were processed with Cell Ranger and analyzed in Seurat for quality control, clustering, and marker gene identification, resulting in 13 cell clusters, with collecting duct principal cells further subclustered into OMCD and IMCD subtypes.

Candidate TFs Selection

We inferred transcriptional regulatory networks in collecting duct principal cells from wild-type mouse kidney snRNA-seq data using the SCENIC pipeline, and prioritized candidate TFs by integrating regulon specificity/activity scores with expression data from IMCD3 cells and CD-PCs based on defined thresholds.

Cell Culture and sgRNA Lentivirus Library Transduction

IMCD3 cells were engineered to stably express dCas9-KRAB via lentiviral transduction and blasticidin selection, followed by transduction with a pooled sgRNA lentiviral library for single-cell CRISPR screening and puromycin selection.

Single-cell CRISPR Library Preparation and Sequencing

We performed single-cell RNA-seq and gRNA detection on dCas9-KRAB IMCD3 cells using the 10x Genomics Chromium platform with Feature Barcode technology, and processed the data with Cell Ranger v7.1.0 and CRISPR Guide Capture Analysis aligned to the mm10 genome.

CRISPR Screening Data Analysis

Gene expression matrices were analyzed with Seurat, cells were filtered and grouped by gRNA identity from Feature Barcode data, and differential expression between perturbation groups was assessed using DESeq2[21].

Enrichment analysis

GO and KEGG enrichment analyses of DEGs were performed using ClusterProfiler in R, with significance determined by BH-adjusted p-values and results visualized using ggplot2. GSEA was performed using MSigDB Hallmark gene sets and DESeq2-normalized expression data, with significance determined by adjusted p-values from 1,000 gene set permutations.

Generation and Validation of Ilf2-Knockdown IMCD3 Cells

A stable Ilf2-knockdown IMCD3 cell line was generated by transducing dCas9-KRAB IMCD3 cells with lentiviruses carrying Ilf2-targeting gRNAs, and knockdown efficiency was validated by qRT-PCR and western blot.

Renal Ischemia-Reperfusion Model

Renal ischemia-reperfusion injury was induced in male mice by clamping the left renal pedicle for 25 minutes under isoflurane anesthesia, followed by 7 days of recovery with analgesia; both ischemic and contralateral kidneys were collected for analysis. See Supplementary Table 8 for ARRIVE reporting.

Bulk RNA sequencing and splicing analysis

Bulk RNA-seq was performed to validate transcriptional effects of Ilf2 knockdown in IMCD3 cells, with differential expression assessed using TPM values and alternative splicing analyzed via SpliceWiz, followed by functional enrichment using ClusterProfiler.

In situ hybridization

Fluorescent in situ hybridization was performed on FFPE kidney sections using RNAscope to detect Ilf2 and Aqp4 transcripts, with imaging acquired by confocal microscopy.

Immunofluorescence Staining

Immunofluorescence staining was performed on kidney sections and cultured IMCD3 cells to detect Ilf2, Aqp2, Ki67, and F-actin, with imaging via confocal microscopy and quantitative analysis of proliferation and multinucleation using QuPath and ImageJ.

Hyperosmotic stress assay

IMCD3 cells were exposed to hyperosmotic stress (600 mOsm/kg) for 12 or 24 hours, and cell viability was assessed via bright-field image analysis using ImageJ2 and by XTT assay to compare control and Ilf2-knockdown conditions.

Statistics

Statistical analyses were performed using GraphPad Prism 10 or R packages. Data are shown as mean ± SD unless stated otherwise. Sample sizes (n) refer to biological replicates and are indicated in figure legends. A P value or adjusted P value < 0.05 was considered statistically significant.

Results

Prediction of TFs in Medullary Collecting Duct Cells

We developed an integrative analysis workflow combining snRNA-seq, regulatory network inference, and TF prioritization to identify key regulators in the medullary collecting duct **(Figure 1a).** We first performed single-nucleus RNA sequencing (snRNA-seq) on dissociated kidneys of wild-type C57BL/6 mice. UMAP analysis and canonical marker expression enabled the identification of major kidney cell types, followed by sub-clustering of collecting duct cells into cortical collecting duct (CCD), medullary collecting duct (MCD; consisting of outer medullary collecting duct, OMCD, and inner medullary collecting duct, IMCD) and deep medullary epithelium (DME) populations **(Figure 1b and c).** We then applied Single-Cell Regulatory Network Inference and Clustering (SCENIC) algorithms[21,22] to infer transcriptional regulatory networks within MCD cells compared to other kidney cell types. This analysis included co-expression-based regulon prediction and motif enrichment analysis, followed by activity scoring using the AUCell approach[21]. To visualize the distribution of TF activity across collecting duct subpopulations, we generated a regulon density plot based on AUCell scores. Regulon density analysis revealed a high regulon density in MCD region, suggesting a particularly robust transcriptional landscape enforcement in this compartment **(Figure 1d).** We next computed for each cell type and TF a Regulon Activity Score (RAS) and Regulon Specificity Score (RSS) (**Supplementary Table S2**)**.** To shortlist candidate TFs that confer the MCD-specific transcriptional landscape for further investigation, we selected regulons associated with a MCD-specific RAS of more than 0.5 and RSS of more than 0.05. In addition, we required a log-normalized average expression of the corresponding TFs of more

than 0.5 (in transcripts per million, TPM) in MCD cells. Additionally, since we intended to utilize a downstream screening approach using the IMCD3 cultured cell model, candidate TFs were selected based on robust mRNA expression in IMCD3 cell bulk RNA-seq, which we defined as TPM >10 in three biological replicates (**Supplementary Table S3**)**.** This resulted in a list of 25 candidate TFs (**Figure 1a, Supplementary Table S1**)**.**

Establishment of a Single-Cell CRISPRi Screening System in IMCD3 Cells

To assay the transcriptomic effects of perturbing these candidate TFs, we devised a single-cell CRISPR interference (CRISPRi) approach in IMCD3 cells. In this system, CRISPRi was used to suppress gene expression in a pooled lentiviral library, followed by single-cell RNA sequencing to assess knockdown efficiency and downstream transcriptional effects of TF perturbation. We first generated IMCD3 cells stably expressing catalytically inactive Cas9 (dCas9) fused to the Krüppel-associated box (KRAB) repressor domain **(Figure 2a and b, Supplementary Figure. S1).** A pooled lentiviral sgRNA library was then introduced into these cells, targeting the 25 prioritized TFs. The library concentration was optimized to target one sgRNA per cell, allowing comparison of the transcriptomic effects induced by each sgRNA in a single experiment. To enhance specificity, the library was designed to contain five different sgRNAs targeting each TF, along with ten non-targeting controls. A capture sequence was embedded into the tracrRNA stem-loop to enable direct sgRNA capture during 10X barcoding[19] without disrupting sgRNA functionality **(Figure 2c and d, Supplementary Figure S3).** As a positive control, we included sgRNAs targeting the known collecting duct TF Grhl2[10].

Following single cell RNA sequencing, library complexity and sgRNA representation were evaluated using the Cell Ranger CRISPR analysis pipeline (v7.1.0), confirming the successful capture of individual gRNAs and sufficient numbers of cells per sgRNA to support downstream functional analyses. Single-cell sequencing data quality was assessed based on the number of detected features (nFeature_RNA), total RNA counts (nCount_RNA), and mitochondrial transcript percentages (percent.mt) **(Supplementary Figure S2).** No significant depletion of cells was observed for any of the targeted TFs, suggesting that none of the selected factors are essential for IMCD3 cell survival under basal conditions **(Figure 2e).**

To evaluate knockdown efficiency, we employed a pseudo-bulk approach: single-cell expression values were normalized and aggregated per perturbation group using log-normalized data in Seurat[23–25]. Differential expression analysis was then performed using DESeq2 by comparing each targeted group against non-targeting controls. Among the 25 targeted TFs, 11 TFs exhibited knockdown efficiencies > 60%, namely Ddit3 (85%), Ehf (76%), Elf3 (83%), Grhl2 (85%), Hdac2 (87%), Hif1a (72%), Ilf2 (89%), Junb (85%), Klf5 (64%), Pole4 (86%), and Xbp1 (91%) **(Figure 2f).**

CRISPRi Screening Reveals Known and Novel TF-Mediated Regulatory Programs

To systematically evaluate the functional consequences of TFs (TFs) knockdown, we performed differential expression analysis on 11 TFs that achieved >60% knockdown efficiency. A pseudo-bulk approach was applied by aggregating single-cell expression profiles within each perturbation group. Differential expression analysis was conducted using DESeq2[26], comparing cells expressing targeting gRNAs to non-targeting controls. Genes with adjusted p-values < 0.05 were considered differentially

expressed (DEGs). Among the 11 TFs, four showed marked transcriptional responses: Grhl2 (1,462 DEGs), Ilf2 (499 DEGs), Junb (69 DEGs), and Klf5 (63 DEGs) **(Figure 3a)**.

Among the TFs analyzed, Grhl2 served as a positive control due to its previously reported role in kidney development, epithelial cell integrity, and renal barrier formation [10,27–29]. Principal component analysis (PCA) revealed clear separation along PC1 (84%) and PC2 (2%) between Grhl2-KD and control cells **(Figure 3b).** Single-cell transcriptomic profiles were further analyzed using Seurat-Mixscape[30]. Heatmap visualization of the differentially expressed genes and up to 200 cells per group, selected and ordered by posterior classification probability, revealed distinct transcriptional signatures between perturbed and control cells. Notably, the expected downregulation of known Grhl2 target genes, including Cldn4, Epcam, Tjp3, Rab25, Gstm2, and Il17re, was observed **(Figure 3c and d, Supplementary Table S4),** consistent with previous studies of this TF[10].

Krüppel-like zinc-finger TF 5 (Klf5) is a well-characterized regulator of cellular proliferation, differentiation[31–33], and survival [34,35]. In the kidney, Klf5 plays essential roles in epithelial integrity, injury response, and repair processes[36–40], and has been linked to tubulointerstitial injury and obstructive nephropathy models[41]. In our screen, Klf5 knockdown induced a moderate transcriptional shift, with PCA showing separation along PC1 (21%) and PC2 (13%) **(Figure 3e).** Heatmap visualization of the differentially expressed genes and up to 200 cells per group revealed clear expression differences **(Figure 3f).** Consistent with previous findings, several genes known to be dependent on Klf5, including Ccnd1[42], Wnt10a[43], Wnt9a[43], Bcam[44,45], Bcar3 and Dusp1[46] were downregulated **(Figure 3g, Supplementary Table S4).**

JunB Proto-Oncogene (Junb), a member of the AP-1 TF complex, is involved in diverse biological processes including development[47–49], cell proliferation[50,51], differentiation[51–53], and immune responses[54,55]. In the kidney, Junb has been previously implicated in fibrotic progression downstream of TGF beta signaling and chronic injury models[56,57]. The knockdown of Junb in our system led to moderate transcriptomic changes, with PCA revealing separation along PC1 (33%) and PC2 (13%) **(Figure 3h).** Heatmap analysis of 200 cells showed widespread expression shifts **(Figure 3i),** including Hmga2[58,59], Ets1[60,61], Cdh2[62], Dab2, and Lcn2[63], all previously associated with Junb-dependent regulation **(Figure 3j, Supplementary Table S4).**

Interleukin enhancer-binding factor 2 (Ilf2) induced extensive transcriptomic changes (499 DEGs) despite limited prior characterization in kidney biology. PCA revealed a strong separation between Ilf2-knockdown and control cells (PC1:42%, PC2:11%) **(Figure 3k),** indicating substantial transcriptional remodeling. Differential expression analysis confirmed widespread changes, and heatmap visualization of 200 cells per group selected and ordered by posterior classification probability in the Seurat Mixscape pipeline, further highlighted the extent of these perturbations **(Figure 3l).** Notably, Ilf2 knockdown led to the downregulation of genes implicated in stress response and proliferation pathways, including Errfi1[64,65], Ier3[66], Bhlhe40[67], Serpine1[68,69], Pdgfb[70,71], and H2afx[72,73] **(Fig. 3m, Supplementary Table S4).** These findings suggest that Ilf2 may control previously unrecognized transcriptional programs in renal epithelial cells, particularly those involved in adaptive stress response.

Functional enrichment analysis of Klf5 and Junb knockdown reveals canonical pathways and novel links to cellular resilience

To assess the functional relevance of the identified TFs, we performed gene ontology enrichment analysis of differentially expressed genes (DEGs). This included Gene Ontology (GO) analysis of biological processes (BP), cellular components (CC), and molecular functions (MF), as well as pathway enrichment based on the Kyoto Encyclopedia of Genes and Genomes (KEGG) database.

Functional enrichment analysis of Junb-dependent DEGs confirmed its established roles in extracellular matrix organization[74,75] and epithelial cell homeastasis[52,76]. Notably, upregulated or downregulated pathways included those associated with ribosomal components and structural molecule activity, suggesting broad alterations in protein synthesis and cytoskeletal integrity **(Figure 4a, Supplementary Table S5).** These pathways may contribute to cellular resilience by modulating biosynthetic and structural programs essential for stress adaptation.

Similarly, GO and KEGG analysis of Klf5-dependent DEGs not only recapitulated its known roles in epithelial maintenance[32,77], apoptotic signaling[78,79] and cell adhesion[77,80,81], but also revealed potential novel functions associated with cellular resilience in renal tubular epithelial cells. These included pathways related to proteolysis regulation, actomyosin organization, and major signaling cascades such as Wnt, mTOR, and Hippo **(Figure 4b, Supplementary Table S5),** which are involved in stress adaptation[82–84], structural integrity[85,86], and regenerative potential[87,88].

Ilf2 maintains IMCD3 cell resilience pathways

Given its more pronounced transcriptomic impact compared to Klf5 and Junb, and the limited understanding of Ilf2's role in kidney biology, we prioritized Ilf2 for further investigation. To gain insight into biological processes potentially regulated by Ilf2, we performed GO and KEGG pathway enrichment analyses on DEGs identified in Ilf2-knockdown IMCD3 cells from the CRISPRi screening dataset. Down-regulated genes covered diverse cellular processes, such as kidney epithelial differentiation, connective tissue and ECM dynamics via proteoglycan and ECM receptor interactions, and RNA polymerase II dependent transcription through core promoter binding. In contrast, genes up-regulated in Ilf2-deficient cells regulate protein synthesis and processing (ribosome biogenesis, cytoplasmic translation), cholesterol biosynthesis, and oxidative phosphorylation. Together, these results suggest that Ilf2 inhibits oxygen- and energy-demanding processes and instead enables cells to build a resilient phenotype by synthesizing mesenchymal gene products such as extracellular components **(Figure 5a, Supplementary Table S5).** GSEA revealed that Ilf2-deficient cells exhibited down-regulation of transcripts associated with TGF-β signaling, hypoxia response signaling, and TNF-α signaling via NF-κB **(Figure 5b, Supplementary Table S5).** These pathways have been implicated in epithelial stress[89,90] and repair capacity in the kidney[91,92], suggesting that Ilf2 may reinforce transcriptional networks underlying renal epithelial resilience.

To validate the findings from our CRISPRi screening, we generated an independent Ilf2 knockdown (Ilf2-KD) cell model using three distinct sgRNAs targeting Ilf2 and three non-targeting sgRNAs, all selected from the original pooled library. Lentiviral transduction was used to introduce the gRNAs into IMCD3-dCas9-KRAB cells, resulting in effective Ilf2 repression. Knockdown efficiency was confirmed by western blot **(Figure 5c and d)** and qPCR analysis **(Figure 5e).** To independently validate the

regulatory impact of Ilf2 depletion, bulk RNA sequencing (RNA-seq) was performed on three non-targeting control samples and three Ilf2-KD samples, each including two independent replicates per sgRNA. Differential gene expression was visualized using a Z-score[93] normalized heatmap **(Figure 5f),** which revealed distinct transcriptional profiles between control and Ilf2-KD groups, with subsets of genes showing upregulation (red) and downregulation (blue).

Importantly, genes associated with key pathways identified in CRISPRi screen also exhibited consistent downregulation in the RNA-seq data, including Serpine1, Pmepa1, Fosl2, Bhlhe40, Farp1, Ier3, Pdgfb, Errfi1, Nasp, Sdc4, H2afx, Large1, Sox4, Sox9, Cux1 and Ext1 **(Figure 5g, Supplementary Table S6, Supplementary Table S4)**. This confirms the robustness of our screening approach and highlights the transcriptional programs regulated by Ilf2.

Ilf2 knockdown alters RNA splicing programs associated with cellular resilience

In addition to transcriptome-wide changes in gene expression, Ilf2 knockdown significantly affected alternative splicing across multiple categories. To systematically assess these effects, we performed differential splicing analysis using the SpliceWiz R package[94], comparing Ilf2-knockdown and control IMCD3 cells. The analysis encompassed seven major splicing event types: alternative 3' splice site (A3SS), alternative 5' splice site (A5SS), alternate first and last exons (AFE, ALE), intron retention (IR), mutually exclusive exons (MXE), and skipped exons (SE). Volcano plot visualization revealed widespread and significant perturbations in splicing patterns following Ilf2 depletion **(Figure 6a),** with skipped exons (SE) representing the most prominently affected category.

Hierarchical clustering of the top 20 differentially spliced events across cells treated with three independent Ilf2 sgRNAs confirmed consistent splicing alterations **(Figure 6b, Supplementary Table S7).** To exemplify these findings, we visualized exon-intron usage in two representative genes: Cortactin (Cttn) and Fyn proto-oncogene (Fyn) **(Figure 6c),** both of which have established roles in kidney pathophysiology. Cttn has been implicated in the regulation of ENaC activity in collecting duct epithelial cells[95], while Fyn has been associated with multiple kidney disease contexts, including fibrosis [96,97], diabetic kidney injury[98,99], and hyperosmotic response[100]. To explore the functional relevance of the splicing changes, we conducted an enrichment analysis on differentially spliced genes. Significant enrichment was observed in pathways related to cytoskeletal organization, junction regulation, and chromatin remodeling, pathways that align with cellular adaptive responses like cytoskeletal dynamics[89], junctional integrity[90], and chromatin remodeling[103] **(Figure 6d, Supplementary Table S7).** Thus, the splicing changes observed upon Ilf2 perturbation likely reflect broader epithelial adaptation mechanisms under stress, suggesting a role for Ilf2 in coordinating structural and epigenetic plasticity through post-transcriptional regulation.

Ilf2 knockdown impairs IMCD3 cell mitosis and resistance to hyperosmotic stress

Functional enrichment of Ilf2-regulated genes at both the expression and splicing levels suggested a role in cellular resilience to stress. To validate these findings and gain mechanistic insight into the biological function of Ilf2, we performed cellular assays in IMCD3 cells. We first assessed cell proliferation. Immunofluorescence staining of the proliferation marker Ki67 showed a mildly reduced proportion of Ki67-

positive cells in Ilf2-KD cells compared to controls **(Figure 7a and b).** Furthermore, DNA-staining analysis identified an increased frequency of multinucleated or abnormally shaped nuclei in Ilf2-KD cells relative to control cells **(Figure 7c and d),** suggesting impaired mitotic regulation. To assess whether Ilf2-KD cells could tolerate hyperosmotic stress, we cultured the cells in a 600 mOsm hyperosmotic medium for 12 and 24 hours. Dying cells were identified using phase-contrast microscopy, based on characteristic morphological features such as a rounded shape, increased cytoplasmic refrigescence, and brighter cell borders[104] **(Figure 7e).** The proportion of dying cells relative to live cells was quantified using automated cell counting in ImageJ **(Figure 7f).** Additionally, cell viability after 12 hours of treatment was measured using an XTT assay. The results demonstrated an increase in the number of dead cells and a decrease in cell viability in Ilf2-KD cells under hyperosmotic conditions **(Figure 7g),** further highlighting Ilf2's involvement in stress resilience.

Expression of Ilf2 in the mouse kidney

Single-nucleus RNA sequencing (snRNA-seq) was used to examine Ilf2 mRNA expression in the collecting duct *in vivo*. Histological analysis of the mouse kidney revealed a gradual increase in Ilf2 expression from the cortex to the medulla, with the highest expression observed in the inner medullary collecting duct (IMCD) segment **(Figure 8a and b).** To validate these findings, we performed *in situ* hybridization using probes targeting Ilf2 and the collecting duct marker Aqp4. Consistent with snRNA-seq results, Ilf2 transcripts were more abundant in the medullary collecting duct than in the cortex and outer medulla **(Figure 8c).** Additionally, immunostaining using antibodies against Ilf2 and the collecting duct marker Aqp2 revealed a similar protein distribution, with Ilf2 protein levels peaking in the IMCD **(Figure 8d).**

Consistently, a re-analysis of bulk RNA-seq data of micro-dissected mouse kidney tissues from cortex, outer medulla, and inner medulla[105] demonstrated enriched expression of Ilf2 in the medullary regions **(Figure 8e).**

Coordinated upregulation of Ilf2, Ilf2-dependent genes, and RNA splicing events in injured kidneys

Given the pronounced effects of Ilf2 knockdown on transcriptional and splicing programs associated with cellular stress responses, we hypothesized that Ilf2 may display differential regulation and activity in settings of kidney injury and repair. To explore this possibility, we examined Ilf2 expression and Ilf2-dependent regulatory targets in a mouse model of ischemia-reperfusion injury (IRI), a well-established system to mimic acute kidney injury and the subsequent regenerative response[106]. We employed a unilateral IRI (uIRI) model in C57BL/6 mice (n = 6). Mice were subjected to uIRI, and kidney tissues were harvested seven days post-injury for imaging and transcriptomic profiling via bulk RNA sequencing **(Figure 9a).** Contralateral non-ischemic kidneys served as controls. Histology indicated signs of tubular injury, inflammatory cell infiltrates, and cast formation in kidneys subjected to uIRI, whereas contralateral kidneys displayed normal histology **(Figure 9b).** Tubular injury scores were significantly higher in ischemic versus contralateral kidneys **(Figure 9c).**

Immunostaining for Ilf2 revealed significantly up-regulated Ilf2 levels in several cell types, including injured proximal tubule and collecting duct cells in post-ischemic versus contralateral kidneys **(Figure 9d).** While Ilf2 signal was strictly restricted to nuclei in control kidneys, Ilf2 protein became detectable in cytoplasm of proximal

tubular and collecting duct cells of kidneys subjected to uIRI, suggesting cytoplasmic translocation of the protein in response to injury **(Figure 9d and e).**

Transcriptomic analyses indicated a significant upregulation of Ilf2 mRNA expression in injured kidneys **(Figure 9f).** In parallel, several transcripts we had found to be down-regulated in Ilf2 knockdown IMCD3 cells were up-regulated in postischemic kidneys, including Bhlhe40, Ext1, Farp1, Fosl2, H2afx, Large1, Nasp, Pdgfb, Pmepa1, Sdc4, Sox4, Cux1, Marveld3, and Serpine1 **(Figure 9f).**

In addition, we observed a number of splicing events that were altered following IRI. Notably, a subset of these events overlapped with alternative splicing events identified in Ilf2 knockdown IMCD3 cells **(Figure 9g, compare to Fig. 6).** One such example is Cttn (cortactin), a gene involved in cell motility, endocytosis, intercellular junction assembly, and cytoskeletal remodeling[107–109], and known to regulate ENaC activity in collecting duct epithelial cells[95]. In IMCD3 cells, Ilf2 knockdown promoted exon skipping in Cttn, whereas in IRI kidney samples, where Ilf2 expression is elevated, Cttn exhibited increased exon inclusion **(Figure 9h).** This inverse splicing pattern is consistent with a potential role of Ilf2 in modulating alternative splicing in response to stress. Together, these findings implicate Ilf2 in postischemic responses of the kidney and suggest an Ilf2-mediated upregulation of cellular resilience, plasticity and stress response programs during epithelial repair.

Discussion

Identifying and functionally characterizing previously unstudied TFs remains a major challenge in molecular biology. Traditional functional studies are time-consuming and labor-intensive, limiting the scale of gene function exploration. Single-cell CRISPR screening has emerged as a powerful tool for high-throughput functional genomics,

enabling systematic interrogation of large gene sets. In this study, we applied bioinformatics strategies combined with single-cell CRISPR interference (CRISPRi) screening to identify novel TFs with functional significance in medullary collecting duct cells (IMCD3).

Our study identifies Ilf2 as a factor with previously uncharacterized regulatory roles in renal tubular epithelial homeostasis. Previous studies on Ilf2 (also known as NF45) have largely focused on its role in cancer biology[110–112], where it functions as a nuclear RNA-binding protein involved in cell cycle progression[111,113,114], mitosis[113,115], biogenesis of ribosomal[116], RNA splicing[110] and DNA damage repair[117,118]. Our results expand this knowledge to kidney epithelial biology. Notably, Ilf2 knockdown in IMCD3 cells led to suppression of canonical pathways including TGF-β signaling, TNF-α/NF-κB signaling, hypoxia response and ribosome organization, all of which are known to be crucial for maintaining tubular cell integrity and responding to injury. These transcriptional perturbations were accompanied by a global disruption of RNA splicing, particularly in genes related to cytoskeletal dynamics, junctional remodeling, and chromatin structure, suggesting a dual role for Ilf2 in both transcriptional and post-transcriptional regulation.

Of particular interest is the observed enrichment of splicing changes in genes involved in cellular architecture and stress responses, such as Fyn, which have previously been linked to kidney injury[99,119], fibrosis[96,97], and hyper-osmolality adaptation[120–122]. The increased prevalence of skipped exons (SE) and other alternative splicing events following Ilf2 depletion indicates a broad regulatory influence on mRNA maturation. Given that NF45 forms a complex with NF90 and participates in spliceosome assembly[116] and RNA stabilization[110,123,124] in other cell

types, it is plausible that Ilf2 exerts similar functions in renal epithelia, particularly under stress.

In vivo, we observed a coordinated upregulation of Ilf2, its predicted downstream targets, and alternative splicing events during the repair phase following ischemia-reperfusion injury (IRI). This temporal expression pattern suggests that Ilf2 orchestrates transcriptomic programs that promote tubular epithelial resilience following acute kidney injury. Importantly, we observed a shift in the cellular localization of Ilf2 following renal ischemia. While Ilf2 protein was restricted to nuclei in uninjured kidneys, it displayed both cytoplasmic and nuclear localization in the epithelial cells of kidneys seven days after IRI. Ilf2, as an RNA-binding protein, has previously been shown to promote IRES-dependent translation of anti-apoptotic proteins like Birc2 (cIAP1), helping cells adapt to ER stress rather than undergoing apoptosis[125]. This raises the possibility that Ilf2 translocation to the cytoplasm might represent an active adaptive mechanism following renal ischemia to promote cellular resilience. In this context, Ilf2 might contribute to renal tubular epithelial injury resistance following an initial episode of renal stress, a phenomenon previously termed “ischemic preconditioning”. Nevertheless, it must be stressed that these possibilities are speculative and require further experimental validation.

In addition to Ilf2, our approach provided further insights into regulatory networks controlled by Grhl2, Klf5, and Junb, all of which have known roles in kidney functions [10,29,37,41,56,126]. Deregulated genes after perturbation of these TFs are consistent with the published literature, but our findings expand observations of these TFs to IMCD3 cells and include novel targets, e.g. Hmga2 and Ets1 as targets of Junb.

In summary, our study establishes Ilf2 as a previously unrecognized regulator of renal tubular cell biology and demonstrates the utility of single-cell CRISPR screening for uncovering context-specific TF functions. Specifically, our data suggest that Ilf2 serves as an integrative regulator of transcriptional and post-transcriptional programs in renal epithelial cells, with particular relevance to cellular resilience. These functions may be critical in the renal medulla, where cells are continuously exposed to extreme osmotic and hypoxic stress, but also in the setting of renal injury. Future studies are warranted to dissect the molecular mechanisms underlying Ilf2-dependent regulation *in vivo* and to explore the potential role of Ilf2 as a therapeutic target in kidney disease.

Disclosure Statement

The authors declare no competing interests.

Data Sharing Statement

Single-cell, single-nuc and bulk RNA sequencing data have been deposited to Gene Expression Omnibus (GEO), accession numbers: GSE299239 (reviewer token onwzwycqtvmntgl), GSE299244 (reviewer token gxibwcquhngpnml), GSE299248 (reviewer token qtklsmwqffwppsz), GSE299251 (reviewer token GSE299251), and GSE299249 (reviewer token edutiqmqxhqxnqp). The primary scripts used for data analysis in this study are publicly available on GitHub at https://github.com/shuangcao-mhh/Perturb-seq-screening-in-IMCD3-cells. Additional research data underlying this work is deposited at the MHH research data server https://doi.org/10.26068/mhhrpm/20250530-000 and can be made available upon request.

Acknowledgments

This project was supported by grants awarded to K.M.S.O: German Research Foundation (DFG) Research Training Group GRK 2318 (B4) – Project ID 318905415. We thank Tatjana Luganskaja, Martina Flechsig, and Gabriele N`Diaye for excellent technical support.

Funding

This project was supported by grants awarded to K.M.S.O: German Research Foundation (DFG) Research Training Group GRK 2318 (B4) – Project ID 318905415, DFG Research Unit 2841, and DFG project 547091997.

Author contributions

SC and KMSO designed the study; SC and KILC conducted experiments; SC, CH analyzed data; SC made the figures; SC drafted the manuscript; KILC, and KMSO edited the manuscript; all authors approved the final version of the manuscript.

References

1. Burg MB, Ferraris JD, Dmitrieva NI. Cellular Response to Hyperosmotic Stresses. *Physiological Reviews*. 2007;87(4):1441-1474. doi:10.1152/physrev.00056.2006

2. Xu S, Huang S, Luan Z, et al. Farnesoid X receptor is essential for the survival of renal medullary collecting duct cells under hypertonic stress. *Proc Natl Acad Sci U S A*. 2018;115(21):5600-5605. doi:10.1073/pnas.1803945115

3. Neuhofer W, Beck FX. Survival in Hostile Environments: Strategies of Renal Medullary Cells. *Physiology*. 2006;21(3):171-180. doi:10.1152/physiol.00003.2006

4. Leiz J, Schmidt-Ott KM. Claudins in the Renal Collecting Duct. *International Journal of Molecular Sciences*. 2020;21(1):221. doi:10.3390/ijms21010221

5. Bonventre JV, Yang L. Cellular pathophysiology of ischemic acute kidney injury. *J Clin Invest*. 2011;121(11):4210-4221. doi:10.1172/JCI45161

6. Heyman SN, Rosenberger C, Rosen S. Experimental ischemia–reperfusion: biases and myths—the proximal vs. distal hypoxic tubular injury debate revisited. *Kidney International*. 2010;77(1):9-16. doi:10.1038/ki.2009.347

7. Jones LM, Chen Y, van Oosten-Hawle P. Redefining proteostasis transcription factors in organismal stress responses, development, metabolism, and health. *Biol Chem*. 2020;401(9):1005-1018. doi:10.1515/hsz-2019-0385

8. Pontoglio M. Hepatocyte Nuclear Factor 1, a Transcription Factor at the Crossroads of Glucose Homeostasis. *Journal of the American Society of Nephrology*. 2000;11(suppl_2):S140. doi:10.1681/ASN.V11suppl_2s140

9. Murray JI, Whitfield ML, Trinklein ND, Myers RM, Brown PO, Botstein D. Diverse and Specific Gene Expression Responses to Stresses in Cultured Human Cells. *Mol Biol Cell*. 2004;15(5):2361-2374. doi:10.1091/mbc.E03-11-0799

10. Hinze C, Ruffert J, Walentin K, et al. GRHL2 Is Required for Collecting Duct Epithelial Barrier Function and Renal Osmoregulation. *JASN*. 2018;29(3):857-868. doi:10.1681/ASN.2017030353

11. Miyakawa H, Woo SK, Dahl SC, Handler JS, Kwon HM. Tonicity-responsive enhancer binding protein, a rel-like protein that stimulates transcription in response to hypertonicity. *Proc Natl Acad Sci U S A*. 1999;96(5):2538-2542. doi:10.1073/pnas.96.5.2538

12. Lee SD, Choi SY, Lim SW, et al. TonEBP stimulates multiple cellular pathways for adaptation to hypertonic stress: organic osmolyte-dependent and -independent pathways. *American Journal of Physiology-Renal Physiology*. 2011;300(3):F707-F715. doi:10.1152/ajprenal.00227.2010

13. Zhang Y, Huang H, Kong Y, et al. Kidney tubular transcription co-activator, Yes-associated protein 1 (YAP), controls the expression of collecting duct aquaporins and water homeostasis. *Kidney International*. 2023;103(3):501-513. doi:10.1016/j.kint.2022.10.007

14. Werth M, Schmidt-Ott KM, Leete T, et al. Transcription factor TFCP2L1 patterns cells in the mouse kidney collecting ducts. Zent R, ed. *eLife*. 2017;6:e24265. doi:10.7554/eLife.24265

15. Hao CM, Yull F, Blackwell T, Kömhoff M, Davis LS, Breyer MD. Dehydration activates an NF-κB–driven, COX2-dependent survival mechanism in renal medullary interstitial cells. *J Clin Invest*. 2000;106(8):973-982.

16. Han Q, Zhang X, Xue R, et al. AMPK Potentiates Hypertonicity-induced Apoptosis by Suppressing NFκB/COX-2 in Medullary Interstitial Cells. *J Am Soc Nephrol*. 2011;22(10):1897-1911. doi:10.1681/ASN.2010080822

17. Hao CM, Redha R, Morrow J, Breyer MD. Peroxisome Proliferator-activated Receptor δ Activation Promotes Cell Survival following Hypertonic Stress*. *Journal of Biological Chemistry*. 2002;277(24):21341-21345. doi:10.1074/jbc.M200695200

18. Bock C, Datlinger P, Chardon F, et al. High-content CRISPR screening. *Nat Rev Methods Primers*. 2022;2(1):1-23. doi:10.1038/s43586-021-00093-4

19. Replogle JM, Norman TM, Xu A, et al. Combinatorial single-cell CRISPR screens by direct guide RNA capture and targeted sequencing. *Nat Biotechnol*. 2020;38(8):954-961. doi:10.1038/s41587-020-0470-y

20. Ghavami S, Pandi A. Chapter Five - CRISPR interference and its applications. In: Singh V, ed. *Progress in Molecular Biology and Translational Science*. Vol 180. Reprogramming the Genome: Applications of CRISPR-Cas in Non-mammalian Systems Part B. Academic Press; 2021:123-140. doi:10.1016/bs.pmbts.2021.01.007

21. Aibar S, González-Blas CB, Moerman T, et al. SCENIC: single-cell regulatory network inference and clustering. *Nat Methods*. 2017;14(11):1083-1086. doi:10.1038/nmeth.4463

22. Van de Sande B, Flerin C, Davie K, et al. A scalable SCENIC workflow for single-cell gene regulatory network analysis. *Nat Protoc*. 2020;15(7):2247-2276. doi:10.1038/s41596-020-0336-2

23. Satija R, Farrell JA, Gennert D, Schier AF, Regev A. Spatial reconstruction of single-cell gene expression data. *Nat Biotechnol*. 2015;33(5):495-502. doi:10.1038/nbt.3192

24. Hao Y, Stuart T, Kowalski MH, et al. Dictionary learning for integrative, multimodal and scalable single-cell analysis. *Nat Biotechnol*. 2024;42(2):293-304. doi:10.1038/s41587-023-01767-y

25. Hao Y, Hao S, Andersen-Nissen E, et al. Integrated analysis of multimodal single-cell data. *Cell*. 2021;184(13):3573-3587.e29. doi:10.1016/j.cell.2021.04.048

26. Love MI, Huber W, Anders S. Moderated estimation of fold change and dispersion for RNA-seq data with DESeq2. *Genome Biol*. 2014;15(12):550. doi:10.1186/s13059-014-0550-8

27. Walentin K, Hinze C, Werth M, et al. A Grhl2-dependent gene network controls trophoblast branching morphogenesis. *Development*. 2015;142(6):1125-1136. doi:10.1242/dev.113829

28. Werth M, Walentin K, Aue A, et al. The transcription factor grainyhead-like 2 regulates the molecular composition of the epithelial apical junctional complex. *Development*. 2010;137(22):3835-3845. doi:10.1242/dev.055483

29. Aue A, Hinze C, Walentin K, et al. A Grainyhead-Like 2/Ovo-Like 2 Pathway Regulates Renal Epithelial Barrier Function and Lumen Expansion. *Journal of the American Society of Nephrology*. 2015;26(11):2704. doi:10.1681/ASN.2014080759

30. Papalexi E, Mimitou EP, Butler AW, et al. Characterizing the molecular regulation of inhibitory immune checkpoints with multimodal single-cell screens. *Nat Genet*. 2021;53(3):322-331. doi:10.1038/s41588-021-00778-2

31. Aksoy I, Giudice V, Delahaye E, et al. Klf4 and Klf5 differentially inhibit mesoderm and endoderm differentiation in embryonic stem cells. *Nat Commun*. 2014;5(1):3719. doi:10.1038/ncomms4719

32. Dong JT, Chen C. Essential role of KLF5 transcription factor in cell proliferation and differentiation and its implications for human diseases. *Cell Mol Life Sci*. 2009;66(16):2691-2706. doi:10.1007/s00018-009-0045-z

33. Liu Y, Wen J kun, Dong L hua, Zheng B, Han M. Krüppel-like factor (KLF) 5 mediates cyclin D1 expression and cell proliferation via interaction with c-Jun in Ang II-induced VSMCs. *Acta Pharmacol Sin*. 2010;31(1):10-18. doi:10.1038/aps.2009.185

34. Zhao Y, Hamza MS, Leong HS, et al. Kruppel-like factor 5 modulates p53-independent apoptosis through Pim1 survival kinase in cancer cells. *Oncogene*. 2008;27(1):1-8. doi:10.1038/sj.onc.1210625

35. Zhu N, Gu L, Findley HW, et al. KLF5 Interacts with p53 in regulating survivin expression in acute lymphoblastic leukemia. *J Biol Chem*. 2006;281(21):14711-14718. doi:10.1074/jbc.M513810200

36. Suzuki N, Kanai A, Suzuki Y, Ogino H, Ochi H. Adrenergic receptor signaling induced by Klf15, a regulator of regeneration enhancer, promotes kidney reconstruction. *Proceedings of the National Academy of Sciences*. 2022;119(33):e2204338119. doi:10.1073/pnas.2204338119

37. Li ZL, Lv LL, Wang B, et al. The profibrotic effects of MK-8617 on tubulointerstitial fibrosis mediated by the KLF5 regulating pathway. *FASEB J*. 2019;33(11):12630-12643. doi:10.1096/fj.201901087RR

38. Mallipattu SK, Estrada CC, He JC. The critical role of Krüppel-like factors in kidney disease. *American Journal of Physiology-Renal Physiology*. 2017;312(2):F259-F265. doi:10.1152/ajprenal.00550.2016

39. Zhang X, Chen J, Lin R, et al. Lactate drives epithelial-mesenchymal transition in diabetic kidney disease via the H3K14la/KLF5 pathway. *Redox Biology*. 2024;75:103246. doi:10.1016/j.redox.2024.103246

40. Li J, Liu L, Zhou WQ, Cai L, Xu ZG, Rane MJ. Roles of Krüppel-like factor 5 in kidney disease. *Journal of Cellular and Molecular Medicine*. 2021;25(5):2342-2355. doi:10.1111/jcmm.16332

41. Fujiu K, Manabe I, Nagai R. Renal collecting duct epithelial cells regulate inflammation in tubulointerstitial damage in mice. *J Clin Invest*. 2011;121(9). doi:10.1172/JCI57582

42. Du JX, Yun CC, Bialkowska A, Yang VW. Protein Inhibitor of Activated STAT1 Interacts with and Up-regulates Activities of the Pro-proliferative Transcription Factor Krüppel-like Factor 5. *J Biol Chem*. 2007;282(7):4782-4793. doi:10.1074/jbc.M603413200

43. Liu Y, Guo B, Aguilera-Jimenez E, et al. Chromatin Looping Shapes KLF5-Dependent Transcriptional Programs in Human Epithelial Cancers. *Cancer Research*. 2020;80(24):5464-5477. doi:10.1158/0008-5472.CAN-20-1287

44. Bourillot PY, Savatier P. Krüppel-like transcription factors and control of pluripotency. *BMC Biol*. 2010;8(1):125. doi:10.1186/1741-7007-8-125

45. Parisi S, Cozzuto L, Tarantino C, et al. Direct targets of Klf5 transcription factor contribute to the maintenance of mouse embryonic stem cell undifferentiated state. *BMC Biology*. 2010;8(1):128. doi:10.1186/1741-7007-8-128

46. Chen C, Benjamin MS, Sun X, et al. KLF5 promotes cell proliferation and tumorigenesis through gene regulationin the TSU-Pr1 human bladder cancer cell line. *International Journal of Cancer*. 2006;118(6):1346-1355. doi:10.1002/ijc.21533

47. JunB can substitute for Jun in mouse development and cell proliferation | Nature Genetics. Accessed February 4, 2025. https://www.nature.com/articles/ng790z

48. Schorpp-Kistner M, Wang Z, Angel P, Wagner EF. JunB is essential for mammalian placentation. *The EMBO Journal*. 1999;18(4):934-948. doi:10.1093/emboj/18.4.934

49. Wilkinson DG, Bhatt S, Ryseck RP, BRAVO R. Tissue-specific expression of c-jun and junB during organogenesis in the mouse. *Development*. 1989;106(3):465-471. doi:10.1242/dev.106.3.465

50. Pérez-Benavente B, Fathinajafabadi A, de la Fuente L, et al. New roles for AP-1/JUNB in cell cycle control and tumorigenic cell invasion via regulation of cyclin E1 and TGF-β2. *Genome Biology*. 2022;23(1):252. doi:10.1186/s13059-022-02800-0

51. Piechaczyk M, Farràs R. Regulation and function of JunB in cell proliferation. *Biochemical Society Transactions*. 2008;36(5):864-867. doi:10.1042/BST0360864

52. Szabowski A, Maas-Szabowski N, Andrecht S, et al. c-Jun and JunB Antagonistically Control Cytokine-Regulated Mesenchymal–Epidermal Interaction in Skin. *Cell*. 2000;103(5):745-755. doi:10.1016/S0092-8674(00)00178-1

53. Katagiri T, Kameda H, Nakano H, Yamazaki S. Regulation of T cell differentiation by the AP-1 transcription factor JunB. *Immunological Medicine*. 2021;44(3):197-203. doi:10.1080/25785826.2021.1872838

54. Ren F jia, Cai X yu, Yao Y, Fang G ying. JunB: a paradigm for Jun family in immune response and cancer. *Front Cell Infect Microbiol*. 2023;13:1222265. doi:10.3389/fcimb.2023.1222265

55. Fontana MF, Baccarella A, Pancholi N, Pufall MA, Herbert DR, Kim CC. JUNB Is a Key Transcriptional Modulator of Macrophage Activation. *The Journal of Immunology*. 2015;194(1):177-186. doi:10.4049/jimmunol.1401595

56. Yao F, Wang X, Cui ZK, et al. ETS2 promotes epithelial-to-mesenchymal transition in renal fibrosis by targeting JUNB transcription. *Laboratory Investigation*. 2020;100(3):438-453. doi:10.1038/s41374-019-0331-9

57. Wernig G, Chen SY, Cui L, et al. Unifying mechanism for different fibrotic diseases. *Proceedings of the National Academy of Sciences of the United States of America*. 2017;114(18):4757. doi:10.1073/pnas.1621375114

58. Nishino J, Kim I, Chada K, Morrison SJ. Hmga2 Promotes Neural Stem Cell Self-Renewal in Young but Not Old Mice by Reducing p16Ink4a and p19Arf Expression. *Cell*. 2008;135(2):227-239. doi:10.1016/j.cell.2008.09.017

59. Vallone D, Battista S, Pierantoni GM, et al. Neoplastic transformation of rat thyroid cells requires the junB and fra-1 gene induction which is dependent on the HMGI-C gene product. *The EMBO Journal*. 1997;16(17):5310-5321. doi:10.1093/emboj/16.17.5310

60. Selvaraj N, Budka JA, Ferris MW, Plotnik JP, Hollenhorst PC. Extracellular Signal-Regulated Kinase Signaling Regulates the Opposing Roles of JUN Family Transcription Factors at ETS/AP-1 Sites and in Cell Migration. *Molecular and Cellular Biology*. 2015;35(1):88-100. doi:10.1128/MCB.00982-14

61. Czuwara-Ladykowska J, Sementchenko VI, Watson DK, Trojanowska M. Ets1 Is an Effector of the Transforming Growth Factor β (TGF-β) Signaling Pathway and an Antagonist of the Profibrotic Effects of TGF-β*. *Journal of Biological Chemistry*. 2002;277(23):20399-20408. doi:10.1074/jbc.M200206200

62. Nguyen HT, Martin LJ. Regulation of Cdh2 by the AP-1 family transcription factor Junb in TM4 Sertoli cells. *Biochem Biophys Res Commun*. 2023;663:32-40. doi:10.1016/j.bbrc.2023.04.078

63. Florin L, Hummerich L, Dittrich BT, et al. Identification of novel AP-1 target genes in fibroblasts regulated during cutaneous wound healing. *Oncogene*. 2004;23(42):7005-7017. doi:10.1038/sj.onc.1207938

64. Cairns J, Fridley BL, Jenkins GD, Zhuang Y, Yu J, Wang L. Differential roles of ERRFI1 in EGFR and AKT pathway regulation affect cancer proliferation. *EMBO reports*. 2018;19(3):e44767. doi:10.15252/embr.201744767

65. Zhao H, Mao H. ERRFI1 exacerbates hepatic ischemia reperfusion injury by promoting hepatocyte apoptosis and ferroptosis in a GRB2-dependent manner. *Mol Med*. 2024;30:82. doi:10.1186/s10020-024-00837-4

66. Arlt A, Schäfer H. Role of the immediate early response 3 (IER3) gene in cellular stress response, inflammation and tumorigenesis. *Eur J Cell Biol*. 2011;90(6-7):545-552. doi:10.1016/j.ejcb.2010.10.002

67. Acosta-Iborra B, Gil-Acero AI, Sanz-Gómez M, et al. Bhlhe40 Regulates Proliferation and Angiogenesis in Mouse Embryoid Bodies under Hypoxia. *Int J Mol Sci*. 2024;25(14):7669. doi:10.3390/ijms25147669

68. Ghosh AK, Vaughan DE. PAI-1 in Tissue Fibrosis. *J Cell Physiol*. 2012;227(2):493-507. doi:10.1002/jcp.22783

69. Czekay RP, Wilkins-Port CE, Higgins SP, et al. PAI-1: An Integrator of Cell Signaling and Migration. *International Journal of Cell Biology*. 2011;2011(1):562481. doi:10.1155/2011/562481

70. Kok HM, Falke LL, Goldschmeding R, Nguyen TQ. Targeting CTGF, EGF and PDGF pathways to prevent progression of kidney disease. *Nat Rev Nephrol*. 2014;10(12):700-711. doi:10.1038/nrneph.2014.184

71. Seifert RA, Alpers CE, Bowen-Pope DF. Expression of platelet-derived growth factor and its receptors in the developing and adult mouse kidney. *Kidney International*. 1998;54(3):731-746. doi:10.1046/j.1523-1755.1998.00046.x

72. Chanoux RA, Yin B, Urtishak KA, Asare A, Bassing CH, Brown EJ. ATR and H2AX Cooperate in Maintaining Genome Stability under Replication Stress*. *Journal of Biological Chemistry*. 2009;284(9):5994-6003. doi:10.1074/jbc.M806739200

73. Dickey JS, Baird BJ, Redon CE, Sokolov MV, Sedelnikova OA, Bonner WM. Intercellular communication of cellular stress monitored by gamma-H2AX induction. *Carcinogenesis*. 2009;30(10):1686-1695. doi:10.1093/carcin/bgp192

74. Maity P, Singh K, Krug L, et al. Persistent JunB activation in fibroblasts disrupts stem cell niche interactions enforcing skin aging. *Cell Reports*. 2021;36(9). doi:10.1016/j.celrep.2021.109634

75. Alfonso-Jaume MA, Bergman MR, Mahimkar R, et al. Cardiac ischemia-reperfusion injury induces matrix metalloproteinase-2 expression through the AP-1 components FosB and JunB. *Am J Physiol Heart Circ Physiol*. 2006;291(4):H1838-1846. doi:10.1152/ajpheart.00026.2006

76. Gervasi M, Bianchi-Smiraglia A, Cummings M, et al. JunB contributes to Id2 repression and the epithelial–mesenchymal transition in response to transforming growth factor–β. *Journal of Cell Biology*. 2012;196(5):589-603. doi:10.1083/jcb.201109045

77. KLF5 promotes breast cancer proliferation, migration and invasion in part by upregulating the transcription of TNFAIP2 | Oncogene. Accessed February 12, 2025. https://www.nature.com/articles/onc2015263

78. Li X, Liu X, Xu Y, et al. KLF5 promotes hypoxia-induced survival and inhibits apoptosis in non-small cell lung cancer cells via HIF-1α. *International Journal of Oncology*. 2014;45(4):1507-1514. doi:10.3892/ijo.2014.2544

79. Yang Y, Goldstein BG, Chao HH, Katz J. KLF4 and KLF5 regulate proliferation, Apoptosis and invasion in esophageal cancer cells. *Cancer Biology & Therapy*. 2005;4(11):1216-1221. doi:10.4161/cbt.4.11.2090

80. Franz H, Rathod M, Zimmermann A, et al. Unbiased screening identifies regulators of cell-cell adhesion and treatment options in pemphigus. *Nat Commun*. 2024;15(1):8044. doi:10.1038/s41467-024-51747-2

81. Liu Y, Chidgey M, Yang VW, Bialkowska AB. Krüppel-like factor 5 is essential for maintenance of barrier function in mouse colon. *Am J Physiol Gastrointest Liver Physiol*. 2017;313(5):G478-G491. doi:10.1152/ajpgi.00172.2017

82. Proud CG. The multifaceted role of mTOR in cellular stress responses. *DNA Repair*. 2004;3(8):927-934. doi:10.1016/j.dnarep.2004.03.012

83. Aramburu J, Ortells MC, Tejedor S, Buxadé M, López-Rodríguez C. Transcriptional regulation of the stress response by mTOR. *Sci Signal*. 2014;7(332):re2. doi:10.1126/scisignal.2005326

84. Mao B, Gao Y, Bai Y, Yuan Z. Hippo signaling in stress response and homeostasis maintenance. *Acta Biochim Biophys Sin (Shanghai)*. 2015;47(1):2-9. doi:10.1093/abbs/gmu109

85. Arnold TR, Stephenson RE, Miller AL. Rho GTPases and actomyosin: Partners in regulating epithelial cell-cell junction structure and function. *Experimental Cell Research*. 2017;358(1):20-30. doi:10.1016/j.yexcr.2017.03.053

86. van Soldt BJ, Cardoso WV. Hippo-Yap/Taz signaling: Complex network interactions and impact in epithelial cell behavior. *WIREs Developmental Biology*. 2020;9(3):e371. doi:10.1002/wdev.371

87. Schunk SJ, Floege J, Fliser D, Speer T. WNT–β-catenin signalling — a versatile player in kidney injury and repair. *Nat Rev Nephrol*. 2021;17(3):172-184. doi:10.1038/s41581-020-00343-w

88. Wang Y, Yu A, Yu FX. The Hippo pathway in tissue homeostasis and regeneration. *Protein Cell*. 2017;8(5):349-359. doi:10.1007/s13238-017-0371-0

89. Miller RL, Kohan DE. Hypoxia regulates endothelin-1 production by the inner medullary collecting duct. *Journal of Laboratory and Clinical Medicine*. 1998;131(1):45-48. doi:10.1016/S0022-2143(98)90076-2

90. Dizin E, Olivier V, Roth I, et al. Activation of the Hypoxia-Inducible Factor Pathway Inhibits Epithelial Sodium Channel–Mediated Sodium Transport in Collecting Duct Principal Cells. *Journal of the American Society of Nephrology*. 2021;32(12):3130. doi:10.1681/ASN.2021010046

91. Higgins DF, Kimura K, Bernhardt WM, et al. Hypoxia promotes fibrogenesis in vivo via HIF-1 stimulation of epithelial-to-mesenchymal transition. *J Clin Invest*. 2007;117(12):3810-3820. doi:10.1172/JCI30487

92. Ding Y, Kim S ll, Lee SY, Koo JK, Wang Z, Choi ME. Autophagy Regulates TGF-β Expression and Suppresses Kidney Fibrosis Induced by Unilateral Ureteral Obstruction. *Journal of the American Society of Nephrology*. 2014;25(12):2835. doi:10.1681/ASN.2013101068

93. Zhao Y, Li MC, Konaté MM, et al. TPM, FPKM, or Normalized Counts? A Comparative Study of Quantification Measures for the Analysis of RNA-seq Data from the NCI Patient-Derived Models Repository. *Journal of Translational Medicine*. 2021;19(1):269. doi:10.1186/s12967-021-02936-w

94. Wong ACH, Wong JJL, Rasko JEJ, Schmitz U. SpliceWiz: interactive analysis and visualization of alternative splicing in R. *Briefings in Bioinformatics*. 2024;25(1):bbad468. doi:10.1093/bib/bbad468

95. Ilatovskaya DV, Pavlov TS, Levchenko V, Negulyaev YA, Staruschenko A. Cortical actin binding protein cortactin mediates ENaC activity via Arp2/3 complex. *FASEB J*. 2011;25(8):2688-2699. doi:10.1096/fj.10-167262

96. Seo HY, Jeon JH, Jung YA, et al. Fyn deficiency attenuates renal fibrosis by inhibition of phospho-STAT3. *Kidney International*. 2016;90(6):1285-1297. doi:10.1016/j.kint.2016.06.038

97. Zhu X, Shi D, Cao K, et al. Sphingosine kinase 2 cooperating with Fyn promotes kidney fibroblast activation and fibrosis via STAT3 and AKT. *Biochimica et Biophysica Acta (BBA) - Molecular Basis of Disease*. 2018;1864(11):3824-3836. doi:10.1016/j.bbadis.2018.09.007

98. Li S, Lin Z, Xiao H, et al. Fyn deficiency inhibits oxidative stress by decreasing c-Cbl-mediated ubiquitination of Sirt1 to attenuate diabetic renal fibrosis. *Metabolism*. 2023;139:155378. doi:10.1016/j.metabol.2022.155378

99. Dorotea D, Jiang S, Pak ES, et al. Pan-Src kinase inhibitor treatment attenuates diabetic kidney injury via inhibition of Fyn kinase-mediated endoplasmic reticulum stress. *Exp Mol Med*. 2022;54(8):1086-1097. doi:10.1038/s12276-022-00810-3

100. Nahm O, Woo SK, Handler JS, Kwon HM. Involvement of multiple kinase pathways in stimulation of gene transcription by hypertonicity. *American Journal of Physiology-Cell Physiology*. 2002;282(1):C49-C58. doi:10.1152/ajpcell.00267.2001

101. Landry J, Huot J. Modulation of actin dynamics during stress and physiological stimulation by a signaling pathway involving p38 MAP kinase and heat-shock protein 27. *Biochem Cell Biol*. 1995;73(9-10):703-707. doi:10.1139/o95-078

102. Lanaspa MA, Almeida NE, Andres-Hernando A, Rivard CJ, Capasso JM, Berl T. The tight junction protein, MUPP1, is up-regulated by hypertonicity and is important in the osmotic stress response in kidney cells. *Proceedings of the National Academy of Sciences*. 2007;104(34):13672-13677. doi:10.1073/pnas.0702752104

103. Johnson AB, Barton MC. Hypoxia-induced and stress-specific changes in chromatin structure and function. *Mutat Res*. 2007;618(1-2):149-162. doi:10.1016/j.mrfmmm.2006.10.007

104. Huh S, Ker DFE, Su H, Kanade T. Apoptosis Detection for Adherent Cell Populations in Time-Lapse Phase-Contrast Microscopy Images. In: Ayache N, Delingette H, Golland P, Mori K, eds. *Medical Image Computing and Computer-Assisted Intervention – MICCAI 2012*. Springer; 2012:331-339. doi:10.1007/978-3-642-33415-3_41

105. Hinze C, Karaiskos N, Boltengagen A, et al. Kidney Single-cell Transcriptomes Predict Spatial Corticomedullary Gene Expression and Tissue Osmolality Gradients. *Journal of the American Society of Nephrology*. 2021;32(2):291. doi:10.1681/ASN.2020070930

106. Hesketh EE, Czopek A, Clay M, et al. Renal Ischaemia Reperfusion Injury: A Mouse Model of Injury and Regeneration. *J Vis Exp*. 2014;(88):51816. doi:10.3791/51816

107. Cosen-Binker LI, Kapus A. Cortactin: The Gray Eminence of the Cytoskeleton. *Physiology*. 2006;21(5):352-361. doi:10.1152/physiol.00012.2006

108. Uruno T, Liu J, Zhang P, et al. Activation of Arp2/3 complex-mediated actin polymerization by cortactin. *Nat Cell Biol*. 2001;3(3):259-266. doi:10.1038/35060051

109. Weaver AM, Karginov AV, Kinley AW, et al. Cortactin promotes and stabilizes Arp2/3-induced actin filament network formation. *Curr Biol*. 2001;11(5):370-374. doi:10.1016/s0960-9822(01)00098-7

110. Marchesini M, Ogoti Y, Fiorini E, et al. ILF2 Is a Regulator of RNA Splicing and DNA Damage Response in 1q21-Amplified Multiple Myeloma. *Cancer Cell*. 2017;32(1):88-100.e6. doi:10.1016/j.ccell.2017.05.011

111. Ni T, Mao G, Xue Q, et al. Upregulated expression of ILF2 in non-small cell lung cancer is associated with tumor cell proliferation and poor prognosis. *J Mol Hist*. 2015;46(4):325-335. doi:10.1007/s10735-015-9624-5

112. Shamanna RA, Hoque M, Pe'ery T, Mathews MB. Induction of p53, p21 and apoptosis by silencing the NF90/NF45 complex in human papilloma virus-transformed cervical carcinoma cells. *Oncogene*. 2013;32(43):5176-5185. doi:10.1038/onc.2012.533

113. Guan D, Altan-Bonnet N, Parrott AM, et al. Nuclear Factor 45 (NF45) Is a Regulatory Subunit of Complexes with NF90/110 Involved in Mitotic Control. *Mol Cell Biol*. 2008;28(14):4629-4641. doi:10.1128/MCB.00120-08

114. Liu X, Zhang C, Qian L, et al. NF45 inhibits cardiomyocyte apoptosis following myocardial ischemia-reperfusion injury. *Pathology - Research and Practice*. 2015;211(12):955-962. doi:10.1016/j.prp.2015.09.018

115. Nourreddine S, Lavoie G, Paradis J, et al. NF45 and NF90 Regulate Mitotic Gene Expression by Competing with Staufen-Mediated mRNA Decay. *Cell Reports*. 2020;31(7):107660. doi:10.1016/j.celrep.2020.107660

116. Wandrey F, Montellese C, Koos K, et al. The NF45/NF90 Heterodimer Contributes to the Biogenesis of 60S Ribosomal Subunits and Influences Nucleolar Morphology. *Molecular and Cellular Biology*. 2015;35(20):3491. doi:10.1128/MCB.00306-15

117. Chiu CL, Li CG, Verschueren E, et al. NUSAP1 Binds ILF2 to Modulate R-Loop Accumulation and DNA Damage in Prostate Cancer. *International Journal of Molecular Sciences*. 2023;24(7):6258. doi:10.3390/ijms24076258

118. Shamanna RA, Hoque M, Lewis-Antes A, et al. The NF90/NF45 Complex Participates in DNA Break Repair via Nonhomologous End Joining ⍰. *Mol Cell Biol*. 2011;31(23):4832-4843. doi:10.1128/MCB.05849-11

119. Uddin MJ, Dorotea D, Pak ES, Ha H. Fyn Kinase: A Potential Therapeutic Target in Acute Kidney Injury. *Biomol Ther (Seoul)*. 2020;28(3):213-221. doi:10.4062/biomolther.2019.214

120. Sheikh-Hamad D, Gustin MC. MAP kinases and the adaptive response to hypertonicity: functional preservation from yeast to mammals. *American Journal of Physiology-Renal Physiology*. 2004;287(6):F1102-F1110. doi:10.1152/ajprenal.00225.2004

121. Zhou X. How do kinases contribute to tonicity-dependent regulation of the transcription factor NFAT5? *World J Nephrol*. 2016;5(1):20-32. doi:10.5527/wjn.v5.i1.20

122. Ferraris JD, Burg MB. Tonicity-dependent regulation of osmoprotective genes in mammalian cells. *Contrib Nephrol*. 2006;152:125-141. doi:10.1159/000096320

123. Haque N, Will A, Cook AG, Hogg JR. A network of DZF proteins controls alternative splicing regulation and fidelity. *Nucleic Acids Research*. 2023;51(12):6411-6429. doi:10.1093/nar/gkad351

124. Wu TH, Shi L, Lowe AW, Nicolls MR, Kao PN. Inducible expression of immediate early genes is regulated through dynamic chromatin association by NF45/ILF2 and NF90/NF110/ILF3. *PLoS One*. 2019;14(4):e0216042. doi:10.1371/journal.pone.0216042

125. Graber TE, Baird SD, Kao PN, Mathews MB, Holcik M. NF45 functions as an IRES trans-acting factor that is required for translation of cIAP1 during the unfolded protein response. *Cell Death Differ*. 2010;17(4):719-729. doi:10.1038/cdd.2009.164

126. Pflegerl P, Vesely P, Hantusch B, et al. Epidermal loss of JunB leads to a SLE phenotype due to hyper IL-6 signaling. *Proceedings of the National Academy of Sciences*. 2009;106(48):20423-20428. doi:10.1073/pnas.0910371106

Legends

Figure 1. Medullary collecting duct cells specific TFs prediction. (a): Workflow for the medullary collecting duct cells TFs selection. **(b):** Uniform Manifold Approximation and Projection (UMAP) utilized to identify major kidney cell types from snRNA-seq of 2 WT mice. Identified types include Collecting Duct Intercalated Cells

(CD-IC), Collecting Duct Principal Cells (CD-PC), Connecting Tubule (CNT), Distal Convoluted Tubule (DCT), Endothelial Cells (ENDO), Parietal Epithelial Cells (PEC), Podocytes (PODO), Proximal Tubule (PT), Thick Ascending Limb (TAL), Thin Limb (TL), and Interstitial Cells (Interst. Cells). **(c):** Identifies sub-clusters within the CD-PC cluster, including Cortical Collecting Duct (CCD1/2), Medullary Collecting Duct (MCD; encompassing Outer Medullary Collecting Duct, OMCD, and Inner Medullary Collecting Duct, IMCD), and Deep Medullary Epithelium (DME). **(d):** Regulon density within CD-PC clusters as inferred by the SCENIC algorithm.

Figure 2. Single cell CRISPRi-based screening pipeline and knockdown validation. (a): Schematic representation of the dCas9-KRAB interference system. **(b):** Lentiviral vector encoding dCas9-KRAB fusion protein. **(c):** sgRNA vector containing a direct-capture sequence inserted into the tracrRNA stem- loop for compatibility with 10X Feature Barcode technology. **(d):** Overview of the single-cell CRISPRi screening strategy using a pooled sgRNA lentiviral library targeting 25 TFs (five sgRNAs per gene) and 10 non-targeting control sgRNAs. **(e):** Numbers of cells transduced by individual sgRNAs targeting the indicated TFs and non-targeting RNAs, confirming sufficient representation for all perturbation conditions. **(f):** Quantification of sgRNA-targeted TF mRNA expression (KD) relative to non-targeting controls (Ctrl). Pseudo-bulk gene expression was calculated using DESeq2, and statistical significance was determined by DESeq2 with Wald test under a negative binomial model, adjusted *P* were computed using the Benjamini-Hochberg method. NS: not significant (adjusted $P > 0.05$), *adjusted $P < 0.05$; ** adjusted $P < 0.01$; *** adjusted $P < 0.001$, **** adjusted $P < 0.0001$.

Figure 3. Recapitulation of known TF targets and discovery of Ilf2-associated regulatory programs. (a): Number of differentially expressed genes (DEGs) identified for each TF using DESeq2 (adjusted p-value < 0.05). Four TFs: Grhl2, Ilf2, Junb, and Klf5 exhibited the most robust transcriptomic effects. **(b,e,h,k):** Principal component analysis (PCA) plots showing transcriptomic separation between TF knockdown samples (five gRNAs per TF) and non-targeting control samples (ten gRNAs), for Grhl2, Klf5, Junb, and Ilf2, respectively. Each point represents the aggregated expression profile of cells targeted by an individual gRNA. Ellipses denote the 95% confidence intervals for each group. **(c,f,i,l):** Heatmaps of log-normalized expression for 200 cells per group selected and ordered by posterior classification probability in the Seurat Mixscape pipeline, illustrating transcriptomic changes upon knockdown of Grhl2, Klf5, Junb, and Ilf2. **(d,g,j,m):** Differential expression of representative target genes following TF knockdown. **(d)** Grhl2-regulated genes, **(g)** Klf5-regulated genes, **(j)** Junb-regulated genes, and **(m)** Ilf2-associated genes involved in stress response and proliferation. Pseudo-bulk differential expression analysis was performed using DESeq2. Gene-wise significance was determined using a Wald test on the negative binomial model, and p-values were adjusted for multiple comparisons using the Benjamini-Hochberg method within DESeq2. * adjusted $P < 0.05$; ** adjusted $P < 0.01$; *** adjusted $P < 0.001$, **** adjusted $P < 0.0001$.

Figure 4. Functional enrichment analysis of differentially expressed genes following Junb and Klf5 knockdown. (a,b): Gene Ontology (GO) and KEGG pathway enrichment analysis of genes significantly down-regulated (left panel) and up-regulated (right panel) upon Junb or Klf5 knockdown (KD). Bars represent significantly enriched functional categories. Categories include GO terms for

Biological Process (BP), Cellular Component (CC), Molecular Function (MF), and KEGG pathways. Numbers indicate the count of genes from the input list associated with each enriched term. Representative gene symbols contributing to the enrichment of each category are listed below the term name. Enrichment was considered significant at adjusted $P < 0.05$ (Benjamini–Hochberg correction).

Figure 5. Transcriptomic analysis of Ilf2 knockdown and confirmation of associated gene expression alterations. (a): Gene Ontology (GO) and KEGG pathway enrichment analysis of genes significantly down-regulated (left panel) and up-regulated (right panel) upon Ilf2 knockdown (KD). Bars represent significantly enriched functional categories. Categories include GO terms for Biological Process (BP), Cellular Component (CC), Molecular Function (MF), and KEGG pathways. Numbers indicate the count of genes from the input list associated with each enriched term. Representative gene symbols contributing to the enrichment of each category are listed below the term name. Enrichment was considered significant at adjusted $P < 0.05$ (Benjamini–Hochberg correction). **(b):** Gene set enrichment plot of selected pathways. The analysis was performed on normalized gene expression data, obtained from DESeq2 along with hallmark gene sets from the Molecular Signature Database (MsigDB). This analysis was performed using GSEA software (Version 4.3.3). A false discovery rate (FDR) threshold of < 0.05 was used to determine significant enrichment. **(c):** Immunoblotting was conducted on cells from three independent knockdown models, using 3 different gRNA (KD1-3). Vinculin (Housekeeping protein) and Ilf2 were detected, verifying the efficacy of the knockdown. **(d):** The intensity of the protein bands was quantified using ImageJ. This quantification involved measuring the signal intensity of the bands to evaluate the relative protein levels in the knockdown versus control cells (Ctrl n=3). A t-test

with Welch's correction was performed on three independent experiments to determine statistical significance. **(e):** Quantitative PCR (qPCR) was performed on the established Ilf2 knockdown IMCD3 cell model using two different non-targeting gRNAs and two Ilf2 gRNAs. Quantification was calculated for both control cells and Ilf2 knockdown cells (n=3). A t-test with Welch's correction was performed on three independent experiments to determine statistical significance. **(f):** Heatmap showing Z-score normalized expression of differentially expressed genes (DEGs) across biological replicates of Ilf2 knockdown (KD) and control (Ctrl) groups from 3 different gRNA mediated Ilf2 knockdowns and controls (n=6). Rows represent genes, while columns represent individual samples. Red indicates upregulated genes, and blue indicates downregulated genes, relative to the mean expression across samples. **(g):** Expression levels of selected genes were analyzed for validation purposes, comparing Ilf2 KD versus Ctrl (n = 6 per group, comprising 3 non-targeting and 3 Ilf2-targeting gRNAs). Expression values were normalized to transcripts per million (TPM) for visualization. Genes shown were selected based on their involvement in the pathways highlighted in **panels a and b**. Differential expression analysis was performed on raw count data using DESeq2, with batch effects adjusted using ComBat-seq. Adjusted p-values were calculated using the Benjamini–Hochberg method to correct for multiple testing.* adjusted $P < 0.05$; ** adjusted $P < 0.01$; *** adjusted $P < 0.001$, **** adjusted $P < 0.0001$.

Figure 6. **Ilf2 knockdown alters alternative splicing patterns and affects gene sets associated with cellular structural and regulatory processes. (a):** Volcano plots showing differential splicing events across seven alternative splicing types in Ilf2-knockdown (KD) versus control (Ctrl) cells, including alternative 3'/5' splice sites (A3SS, A5SS), alternate first/last exon usage (AFE, ALE), intron retention (IR),

mutually exclusive exons (MXE), and skipped exons (SE). The x-axis indicates $\log_2$ fold change in event inclusion; the y-axis indicates $-\log_{10}$(FDR). Multiple testing correction was performed using the Benjamini–Hochberg correction to determine statistical significance. In the plot, genes with an adjusted $P < 0.05$ and a $\log_2$ fold change > 1 were considered significant. Selected genes are labeled in red (compare to Fig. 9 below). **(b):** Heatmap of the top 20 most significantly altered splicing events, based on PSI (Percent Spliced-In) values. Rows indicate biological replicates, columns represent individual events; red and blue denote higher and lower inclusion levels, respectively. **(c):** Representative examples of alternative splicing changes in Cttn and Fyn. Coverage plots display normalized read densities across the Cttn (chr7:144.003–144.006 Mb) and Fyn (chr10:39404–39408 Mb) gene loci. Each curve represents the mean normalized coverage across replicates for each condition: control (red) and KD (blue). Shaded areas indicate the standard error. Transcript isoforms are shown below with exon–intron structures. **(d):** Enrichment Combined GO and KEGG pathway enrichment analysis of genes with significantly altered splicing events. The top 5 enriched terms from each group are shown (adjusted $P < 0.05$, Benjamini–Hochberg correction). Numbers indicate the count of genes from the input list associated with each enriched term. Representative gene symbols contributing to the enrichment of each category are listed below the term name.

Figure 7. Ilf2 biological roles in IMCD3 cells. (a): Ki67 staining in cells transduced with two different Ilf2-targeting gRNAs (Ilf2 knockdown, KD1–2) and two non-targeting control gRNAs (Ctrl1–2). DAPI (blue) was used as a nuclear counterstain, Ki67 was labeled in pink, and F-actin (green) was used to delineate cell boundaries. **(b):** Quantification of Ki67 positive cells ratio in one culture well, each dot represent an independent well (gRNA pair 1 n=7, gRNA pair 2 n=10). Statistical significance

between control and knockdown groups was assessed using two-way ANOVA followed by Bonferroni-corrected pairwise comparisons. **(c):** DAPI staining of the Ilf2 knockdown cells and control cells, F-actin was stained for the cell border detection. Multi-nucleus cells were pointed out with arrows. **(d):** Quantification of the multi-nucleated cells, each dot represents an independent culture well. The analysis included two different gRNA pairs (gRNA pair 1 n=4, gRNA pair 2 n=4). Statistical significance between control and knockdown groups was assessed using two-way ANOVA followed by Bonferroni-corrected pairwise comparisons. **(e):** Representative phase-contrast images of Ilf2 knockdown and control IMCD3 cells after 12-hour exposure to 600 mOsm hyperosmotic medium. Dying cells exhibit characteristic morphological changes, including a rounded shape, increased cytoplasmic refringence (bright border), and detachment from the culture surface. **(f):** Quantification of dead cells relative to living cells was performed in ImageJ. Each dot represents an independent well (n=3 for each time point per condition). Statistical significance between control and knockdown groups was assessed using two-way ANOVA followed by Bonferroni-corrected pairwise comparisons. **(g):** Quantification of cell viability under isotonic or hyperosmotic conditions by measuring the absorbance with XTT assay. Each dot represents an independent well (2 pairs of gRNA were quantified separately, gRNA pair 1 n=8, gRNA pair 2 n=8). Tukey's multiple comparisons test was used to access the statistical significance. * adjusted $P < 0.05$; ** adjusted $P < 0.01$; *** adjusted $P < 0.001$.

Fig8. Expression profile of Ilf2 RNA and protein in the mouse collecting duct. (a): sn-seq UMAP plot of sub-clustered collecting duct cells, featuring the expression of the Ilf2 gene, the expression level was log-normalized with the Seurat data processing package. **(b):** Schematic illustration of nephron tubules and the RNA

expression level of the Ilf2 as shown in purple. **(c):** In situ hybridization (ISH) was performed on 2 WT mouse kidney slices (n=2) to visualize Ilf2 mRNA expression. Samples were stained with DAPI and labeled for Aqp4 (A marker of collecting duct principal cells) and Ilf2. Representative images from the cortex, outer medulla, and inner medulla regions are displayed to illustrate the distribution of Ilf2 mRNA levels within the kidney collecting duct. Zoomed-in images of selected regions were supplied on the right side. **(d):** Immunofluorescence (IF) staining was performed on 2 WT mouse kidney slices (n=2) to visualize Ilf2 protein expression. Samples were stained with DAPI, mouse anti-Aqp2 (A marker of collecting duct principal cells), and mouse anti-Ilf2. Representative images from the cortex, outer medulla, and inner medulla regions are displayed to illustrate the distribution of Ilf2 protein levels within the kidney collecting duct. Zoomed-in images of selected regions were supplied on the right side. **(e):** Bulk RNA-seq data from cortex, outer medulla, and inner medulla regions of the mouse kidney were reanalyzed to assess Ilf2 expression levels. The data were obtained from a previously published study by our group[105]. The expression was normalized to transcripts per million (TPM). Statistical significance was assessed using Welch's ANOVA with Brown–Forsythe correction, appropriate for datasets with unequal variances across groups. NS: not significant (adjusted $P > 0.05$), ** adjusted $P < 0.01$.

Figure 9. Ilf2 relevant genes expression in IRI mouse model. **(a):** Schematic representation of the experimental workflow, unilateral ischemia reperfusion injury (uIRI) was utilized, contralateral (Ctrl) and injured (IRI) kidney samples were sequenced (bulk RNAseq) 7 days post-injury. **(b):** Representative kidney sections from Ctrl and IRI mice at day 7 post-injury were stained with PAS to assess tubular morphology and basement membrane integrity. **(c):** Kidney injury marker gene

(Havcr1) expression at Day7. Each dot represents an individual mouse, n=6 per group. Statistical significance was assessed using a t-test with Welch's correction between Ctrl and IRI samples. **(d):** Immunofluorescence staining was performed on kidney sections from 5 contralateral control (Ctrl) and 5 ischemia-reperfusion injury (IRI) mice (n = 5 per group) to assess Ilf2 protein expression. Sections were stained with DAPI (nuclei), mouse anti-Aqp2 (collecting duct marker), mouse anti-Ilf2, and Lotus Tetragonolobus Lectin (LTL, proximal tubule brush border marker). Representative images from the cortex and medulla are shown. Under IRI conditions, increased Ilf2 expression and subcellular redistribution from the nucleus to the cytoplasm were observed. Insets highlight Ilf2 translocation in magnified views. **(e):** Quantification of Ilf2 expression across all cell types and within the nucleus and cytoplasm of proximal tubule (PT) cells. The signal intensity of individual cells was measured using QuPath software. For each sample, the mean signal intensity was calculated across all detected cells or specifically within PT cells. The cytoplasmic region was defined as a 5 µm-wide area surrounding each identified nucleus. Each dot represents one independent kidney sample. Statistical significance was assessed by Mann-Whitney U test. **(f):** Genes downregulated upon Ilf2 knockdown exhibit upregulation in the injured kidney, including Ilf2. Each dot represents an individual mouse, n=6 per group. Statistical significance was assessed using a t-test with Welch's correction between Ctrl and IRI samples. **(g):** Volcano plots showing differentially spliced events in skipped exons (SE) category in IRI compared to control kidneys. The x-axis indicates $\log_2$ fold change in splicing event inclusion; the y-axis indicates $-\log_{10}$(FDR). Red dots and gene name (red) highlight splicing events that overlap with those observed in Ilf2-knockdown IMCD3 cells (compare to Fig. 6). Multiple testing correction was performed using the Benjamini–Hochberg correction

to determine statistical significance. In the plot, genes with an adjusted p-value < 0.05 and a $\log_2$ fold change > 1 were considered significant. **(h):** Representative alternative spliced gene Cttn inclusion in IRI samples. Coverage plots display normalized read densities across the Cttn (chr7:144.003–144.006 Mb) gene loci. Each curve represents the mean normalized coverage across replicates for each condition: Ctrl (red) and IRI (blue). Shaded areas indicate the standard error. Transcript isoforms are shown below with exon–intron structures. * adjusted $P < 0.05$; ** adjusted $P < 0.01$; *** adjusted $P < 0.001$, **** adjusted $P < 0.0001$

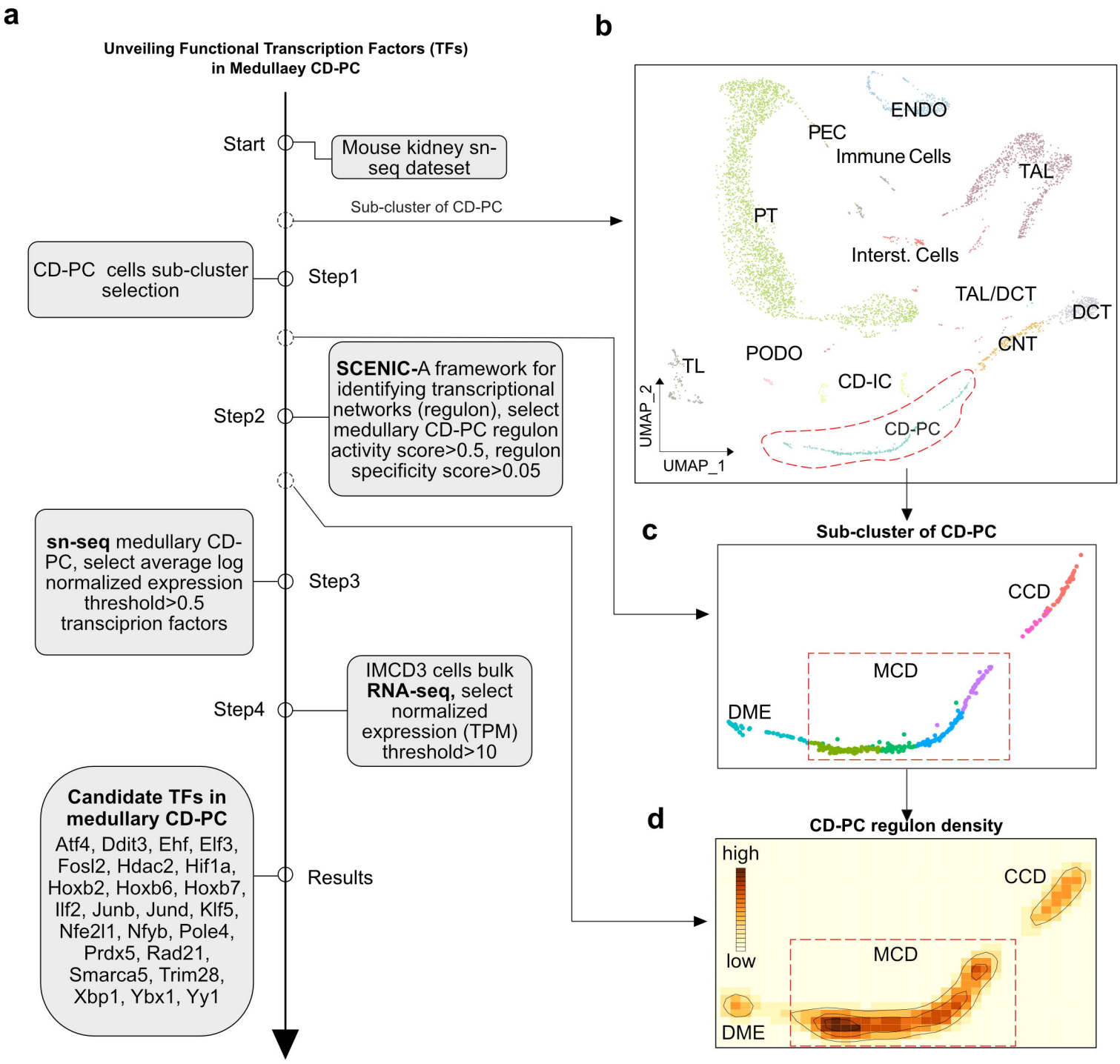
a
Unveiling Functional Transcription Factors (TFs) in Medullaey CD-PC
Start
Mouse kidney sn-seq dateset
Sub-cluster of CD-PC
CD-PC cells sub-cluster selection
Step1
SCENIC-A framework for identifying transcriptional networks (regulon), select medullary CD-PC regulon activity score>0.5, regulon specificity score>0.05
Step2
sn-seq medullary CD-PC, select average log normalized expression threshold>0.5 transciprion factors
Step3
IMCD3 cells bulk RNA-seq, select normalized expression (TPM) threshold>10
Step4
Candidate TFs in medullary CD-PC
Atf4, Ddit3, Ehf, Elf3, Fosl2, Hdac2, Hif1a, Hoxb2, Hoxb6, Hoxb7, Ilf2, Junb, Jund, Klf5, Nfe2l1, Nfyb, Pole4, Prdx5, Rad21, Smarca5, Trim28, Xbp1, Ybx1, Yy1
Results
b
ENDO
PEC
Immune Cells
TAL
PT
Interst. Cells
TAL/DCT
DCT
CNT
PODO
TL
CD-IC
CD-PC
UMAP_2
UMAP_1
c
Sub-cluster of CD-PC
CCD
MCD
DME
d
CD-PC regulon density
high
low
CCD
MCD
DME

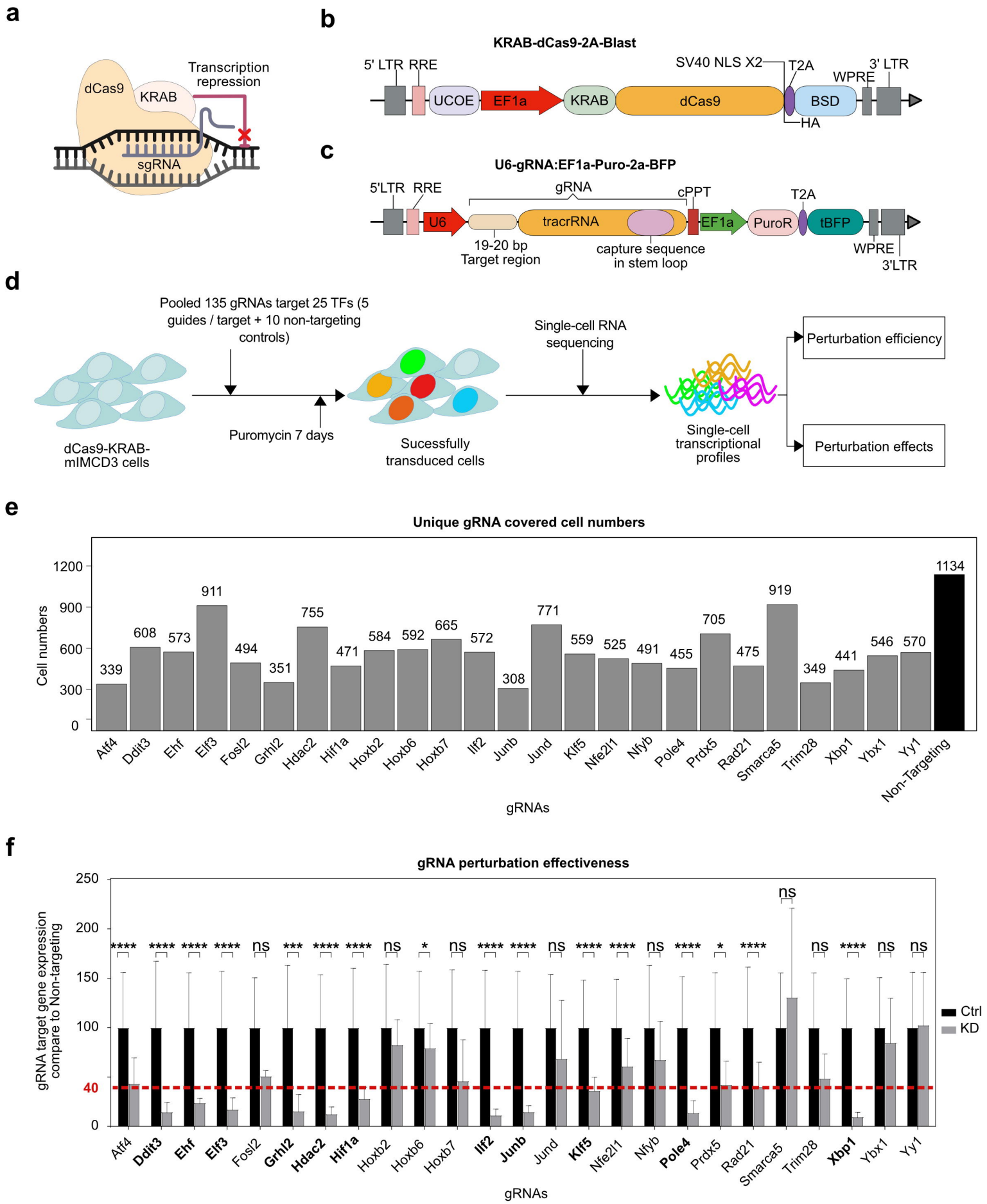
a
dCas9
KRAB
Transcription repression
sgRNA
b
KRAB-dCas9-2A-Blast
5' LTR
RRE
UCOE
EF1a
KRAB
dCas9
SV40 NLS X2
T2A
HA
BSD
WPRE
3' LTR
c
U6-gRNA:EF1a-Puro-2a-BFP
5'LTR
RRE
U6
gRNA
19-20 bp Target region
tracrRNA
capture sequence in stem loop
cPPT
EF1a
T2A
PuroR
tBFP
WPRE
3'LTR
d
Pooled 135 gRNAs target 25 TFs (5 guides / target + 10 non-targeting controls)
dCas9-KRAB-mIMCD3 cells
Puromycin 7 days
Sucessfully transduced cells
Single-cell RNA sequencing
Single-cell transcriptional profiles
Perturbation efficiency
Perturbation effects
e
Unique gRNA covered cell numbers
Cell numbers
0
300
600
900
1200
339
608
573
911
494
351
755
471
584
592
665
572
308
771
559
525
491
455
705
475
919
349
441
546
570
1134
Atf4
Ddit3
Ehf
Elf3
Fosl2
Grhl2
Hdac2
Hif1a
Hoxb2
Hoxb6
Hoxb7
Ilf2
Junb
Jund
Klf5
Nfe2l1
Nfyb
Pole4
Prdx5
Rad21
Smarca5
Trim28
Xbp1
Ybx1
Yy1
Non-Targeting
gRNAs
f
gRNA perturbation effectiveness
gRNA target gene expression compare to Non-targeting
0
40
100
150
200
250
**** **** **** **** ns *** **** **** ns * ns **** **** ns **** **** ns **** * **** ns ns **** ns ns
Ctrl
KD
Atf4
Ddit3
Ehf
Elf3
Fosl2
Grhl2
Hdac2
Hif1a
Hoxb2
Hoxb6
Hoxb7
Ilf2
Junb
Jund
Klf5
Nfe2l1
Nfyb
Pole4
Prdx5
Rad21
Smarca5
Trim28
Xbp1
Ybx1
Yy1
gRNAs

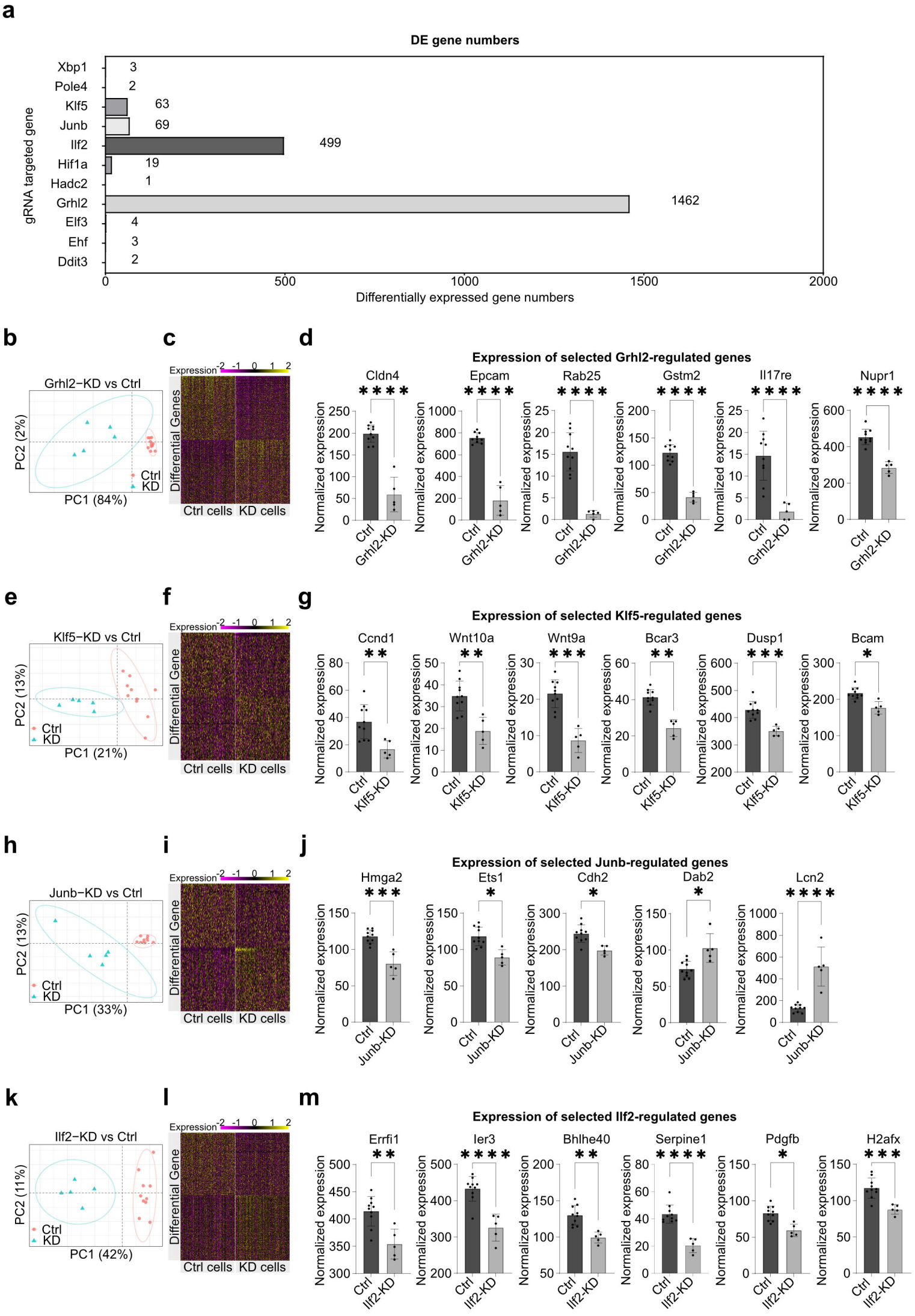
a
DE gene numbers
gRNA targeted gene
Xbp1 3
Pole4 2
Klf5 63
Junb 69
Ilf2 499
Hif1a 19
Hadc2 1
Grhl2 1462
Elf3 4
Ehf 3
Ddit3 2
0 500 1000 1500 2000
Differentially expressed gene numbers
b
Grhl2−KD vs Ctrl
PC2 (2%)
PC1 (84%)
Ctrl
KD
c
Expression -2 -1 0 1 2
Differential Genes
Ctrl cells KD cells
d
Expression of selected Grhl2-regulated genes
Cldn4 Epcam Rab25 Gstm2 Il17re Nupr1
Normalized expression
Ctrl Grhl2-KD
e
Klf5−KD vs Ctrl
PC2 (13%)
PC1 (21%)
Ctrl
KD
f
Expression -2 -1 0 1 2
Differential Gene
Ctrl cells KD cells
g
Expression of selected Klf5-regulated genes
Ccnd1 Wnt10a Wnt9a Bcar3 Dusp1 Bcam
Normalized expression
Ctrl Klf5-KD
h
Junb−KD vs Ctrl
PC2 (13%)
PC1 (33%)
Ctrl
KD
i
Expression -2 -1 0 1 2
Differential Gene
Ctrl cells KD cells
j
Expression of selected Junb-regulated genes
Hmga2 Ets1 Cdh2 Dab2 Lcn2
Normalized expression
Ctrl Junb-KD
k
Ilf2−KD vs Ctrl
PC2 (11%)
PC1 (42%)
Ctrl
KD
l
Expression -2 -1 0 1 2
Differential Gene
Ctrl cells KD cells
m
Expression of selected Ilf2-regulated genes
Errfi1 Ier3 Bhlhe40 Serpine1 Pdgfb H2afx
Normalized expression
Ctrl Ilf2-KD

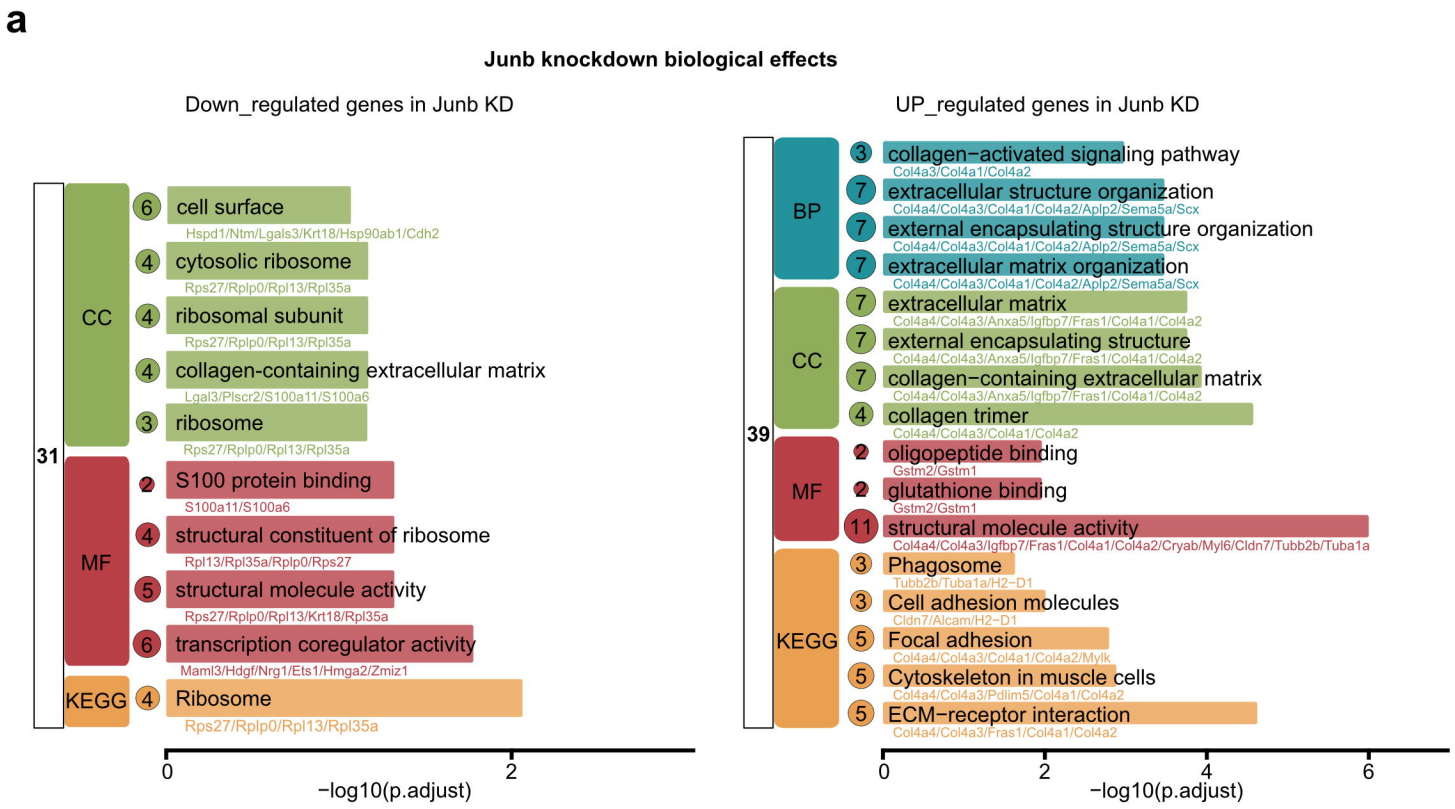
a
Junb knockdown biological effects
Down_regulated genes in Junb KD
UP_regulated genes in Junb KD
31
CC
6 cell surface
Hspd1/Ntm/Lgals3/Krt18/Hsp90ab1/Cdh2
4 cytosolic ribosome
Rps27/Rplp0/Rpl13/Rpl35a
4 ribosomal subunit
Rps27/Rplp0/Rpl13/Rpl35a
4 collagen-containing extracellular matrix
Lgal3/Plscr2/S100a11/S100a6
3 ribosome
Rps27/Rplp0/Rpl13/Rpl35a
MF
2 S100 protein binding
S100a11/S100a6
4 structural constituent of ribosome
Rpl13/Rpl35a/Rplp0/Rps27
5 structural molecule activity
Rps27/Rplp0/Rpl13/Krt18/Rpl35a
6 transcription coregulator activity
Maml3/Hdgf/Nrg1/Ets1/Hmga2/Zmiz1
KEGG
4 Ribosome
Rps27/Rplp0/Rpl13/Rpl35a
0
2
−log10(p.adjust)
39
BP
3 collagen−activated signaling pathway
Col4a3/Col4a1/Col4a2
7 extracellular structure organization
Col4a4/Col4a3/Col4a1/Col4a2/Aplp2/Sema5a/Scx
7 external encapsulating structure organization
Col4a4/Col4a3/Col4a1/Col4a2/Aplp2/Sema5a/Scx
7 extracellular matrix organization
Col4a4/Col4a3/Col4a1/Col4a2/Aplp2/Sema5a/Scx
CC
7 extracellular matrix
Col4a4/Col4a3/Anxa5/Igfbp7/Fras1/Col4a1/Col4a2
7 external encapsulating structure
Col4a4/Col4a3/Anxa5/Igfbp7/Fras1/Col4a1/Col4a2
7 collagen−containing extracellular matrix
Col4a4/Col4a3/Anxa5/Igfbp7/Fras1/Col4a1/Col4a2
4 collagen trimer
Col4a4/Col4a3/Col4a1/Col4a2
MF
2 oligopeptide binding
Gstm2/Gstm1
2 glutathione binding
Gstm2/Gstm1
11 structural molecule activity
Col4a4/Col4a3/Igfbp7/Fras1/Col4a1/Col4a2/Cryab/Myl6/Cldn7/Tubb2b/Tuba1a
KEGG
3 Phagosome
Tubb2b/Tuba1a/H2−D1
3 Cell adhesion molecules
Cldn7/Alcam/H2−D1
5 Focal adhesion
Col4a4/Col4a3/Col4a1/Col4a2/Mylk
5 Cytoskeleton in muscle cells
Col4a4/Col4a3/Pdlim5/Col4a1/Col4a2
5 ECM−receptor interaction
Col4a4/Col4a3/Fras1/Col4a1/Col4a2
0
2
4
6
−log10(p.adjust)
b
Klf5 knockdown biological effects
Down_regulated genes in Klf5 KD
Up_regulated genes in Klf5 KD
33
BP
5 cell−matrix adhesion
Bcam/Cdk6/Msln/S100a10/Wnt4
5 actomyosin structure organization
Ect2/Epb41l4a/Krt19/S100a10/Wnt4
7 epithelial cell differentiation
Ccnd1/Cdk6/Klf5/Krt19/Krt7/Wnt4/Wnt9a
7 regulation of proteolysis
Bok/Cryab/Nupr1/S100a10/Timp2/Wfdc2/Wnt9a
9 regulation of hydrolase activity
Bcar3/Bok/Cryab/Ect2/S100a10/Timp2/Wfdc2/Wnt4/Wnt9a
CC
2 M band
Cryab/Hspb1
7 cell surface
Bcam/Cryab/Lmo7/Msln/S100a10/Timp2/Wnt4
MF
3 frizzled binding
Wnt10a/Wnt4/Wnt9a
KEGG
3 mTOR signaling pathway
Wnt10a/Wnt4/Wnt9a
3 Signaling pathways regulating pluripotency of stem cells
Wnt10a/Wnt4/Wnt9a
4 Wnt signaling pathway
Ccnd1/Wnt10a/Wnt4/Wnt9a
4 Hippo signaling pathway
Ccnd1/Wnt10a/Wnt4/Wnt9a
0
2
−log10(p.adjust)
30
BP
6 cell growth
Bdnf/Fn1/Gas1/Ptprj/Sema5a/Sorbs2
4 regulation of chemotaxis
Csf1/Fn1/Ptprj/Sema5a
6 mononuclear cell differentiation
Csf1/Cyp26b1/Itgb8/Ptprj/Tmem176a/Tmem176b
4 positive regulation of chemotaxis
Csf1/Fn1/Ptprj/Sema5a
5 cell−matrix adhesion
Csf1/Fn1/Itgb8/Pkhd1/Ptprj
CC
5 apical part of cell
Abcc4/Fn1/Igfbp2/Pkhd1/Sorbs2
6 cell surface
Abcc4/Adgrg6/Anxa5/Cp/Itgb8/Ptprj
5 apical plasma membrane
Abcc4/Fn1/Igfbp2/Pkhd1/Sorbs2
MF
2 heparan sulfate proteoglycan binding
Fst/Sema5a
4 glycosaminoglycan binding
Adamts5/Aplp2/Fn1/Sema5a
5 sulfur compound binding
Adamts5/Aplp2/Fn1/Fst/Sema5a
3 proteoglycan binding
Fn1/Fst/Sema5a
6 signaling receptor regulator activity
Bdnf/Csf1/Fn1/Fst/Igfbp2/Sema5a
0
2
−log10(p.adjust)

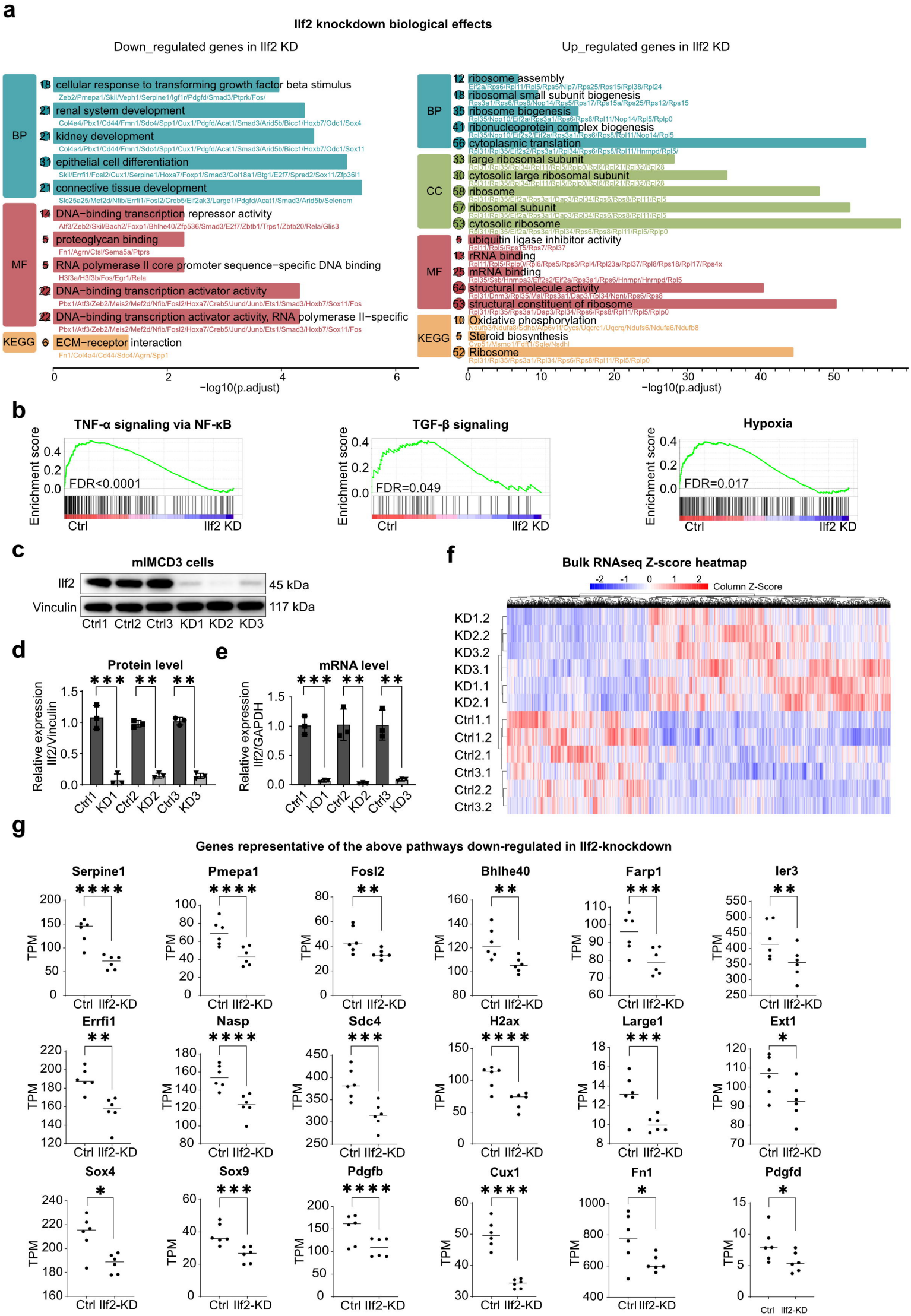
a
Ilf2 knockdown biological effects
Down_regulated genes in Ilf2 KD
Up_regulated genes in Ilf2 KD
BP
18 cellular response to transforming growth factor beta stimulus
Zeb2/Pmepa1/Skil/Veph1/Serpine1/Igf1r/Pdgfd/Smad3/Ptprk/Fos/
21 renal system development
Col4a4/Pbx1/Cd44/Fmn1/Sdc4/Spp1/Cux1/Pdgfd/Acat1/Smad3/Arid5b/Bicc1/Hoxb7/Odc1/Sox4
21 kidney development
Col4a4/Pbx1/Cd44/Fmn1/Sdc4/Spp1/Cux1/Pdgfd/Acat1/Smad3/Arid5b/Bicc1/Hoxb7/Odc1/Sox11
31 epithelial cell differentiation
Skil/Errfi1/Fosl2/Cux1/Serpine1/Hoxa7/Foxp1/Smad3/Col18a1/Btg1/E2f7/Spred2/Sox11/Zfp36l1
21 connective tissue development
Slc25a25/Mef2d/Nfib/Errfi1/Fosl2/Creb5/Eif2ak3/Large1/Pdgfd/Acat1/Smad3/Arid5b/Selenom
MF
14 DNA−binding transcription repressor activity
Atf3/Zeb2/Skil/Bach2/Foxp1/Bhlhe40/Zfp536/Smad3/E2f7/Zbtb1/Trps1/Zbtb20/Rela/Glis3
5 proteoglycan binding
Fn1/Agrn/Ctsl/Sema5a/Ptprs
5 RNA polymerase II core promoter sequence−specific DNA binding
H3f3a/H3f3b/Fos/Egr1/Rela
22 DNA−binding transcription activator activity
Pbx1/Atf3/Zeb2/Meis2/Mef2d/Nfib/Fosl2/Hoxa7/Creb5/Jund/Junb/Ets1/Smad3/Hoxb7/Sox11/Fos
22 DNA−binding transcription activator activity, RNA polymerase II−specific
Pbx1/Atf3/Zeb2/Meis2/Mef2d/Nfib/Fosl2/Hoxa7/Creb5/Jund/Junb/Ets1/Smad3/Hoxb7/Sox11/Fos
KEGG
6 ECM−receptor interaction
Fn1/Col4a4/Cd44/Sdc4/Agrn/Spp1
0 2 4 6
−log10(p.adjust)
BP
12 ribosome assembly
Eif2a/Rps6/Rpl11/Rpl5/Rps5/Nip7/Rps25/Rps15/Rpl38/Rpl24
18 ribosomal small subunit biogenesis
Rps3a1/Rps6/Rps8/Nop14/Rps5/Rps17/Rps15a/Rps25/Rps12/Rps15
35 ribosome biogenesis
Rpl35/Nop10/Eif2a/Rps3a1/Rps6/Rps8/Rpl11/Nop14/Rpl5/Rplp0
41 ribonucleoprotein complex biogenesis
Rpl35/Nop10/Eif2s2/Eif2a/Rps3a1/Rps6/Rps8/Rpl11/Nop14/Rpl5
56 cytoplasmic translation
Rpl31/Rpl35/Eif2s2/Rps3a1/Rpl34/Rps6/Rps8/Rpl11/Hnrnpd/Rpl5/
33 large ribosomal subunit
Rpl31/Rpl35/Rpl34/Rpl11/Rpl5/Rplp0/Rpl6/Rpl21/Rpl32/Rpl28
30 cytosolic large ribosomal subunit
Rpl31/Rpl35/Rpl34/Rpl11/Rpl5/Rplp0/Rpl6/Rpl21/Rpl32/Rpl28
58 ribosome
Rpl31/Rpl35/Eif2a/Rps3a1/Dap3/Rpl34/Rps6/Rps8/Rpl11/Rpl5
57 ribosomal subunit
Rpl31/Rpl35/Eif2a/Rps3a1/Dap3/Rpl34/Rps6/Rps8/Rpl11/Rpl5
53 cytosolic ribosome
Rpl31/Rpl35/Eif2a/Rps3a1/Rpl34/Rps6/Rps8/Rpl11/Rpl5/Rplp0
MF
5 ubiquitin ligase inhibitor activity
Rpl11/Rpl5/Rps15/Rps7/Rpl37
13 rRNA binding
Rpl11/Rpl5/Rplp0/Rpl6/Rps5/Rps3/Rpl4/Rpl23a/Rpl37/Rpl8/Rps18/Rpl17/Rps4x
25 mRNA binding
Rpl35/Ssb/Hnrnpa3/Eif2s2/Eif2a/Rps3a1/Rps6/Hnrnpr/Hnrnpd/Rpl5
64 structural molecule activity
Rpl31/Dnm3/Rpl35/Mal/Rps3a1/Dap3/Rpl34/Npnt/Rps6/Rps8
53 structural constituent of ribosome
Rpl31/Rpl35/Rps3a1/Dap3/Rpl34/Rps6/Rps8/Rpl11/Rpl5/Rplp0
KEGG
10 Oxidative phosphorylation
Ndufb3/Ndufa6/Sdhb/Atp6v1f/Cycs/Uqcrc1/Uqcrq/Ndufs6/Ndufa6/Ndufb8
5 Steroid biosynthesis
Cyp51/Msmo1/Fdft1/Sqle/Nsdhl
52 Ribosome
Rpl31/Rpl35/Rps3a1/Rpl34/Rps6/Rps8/Rpl11/Rpl5/Rplp0
0 10 20 30 40 50
−log10(p.adjust)
b
TNF-α signaling via NF-κB
Enrichment score
FDR<0.0001
Ctrl
Ilf2 KD
TGF-β signaling
FDR=0.049
Hypoxia
FDR=0.017
c
mIMCD3 cells
Ilf2
45 kDa
Vinculin
117 kDa
Ctrl1 Ctrl2 Ctrl3 KD1 KD2 KD3
d
Protein level
Relative expression Ilf2/Vinculin
e
mRNA level
Relative expression Ilf2/GAPDH
f
Bulk RNAseq Z-score heatmap
Column Z-Score
KD1.2
KD2.2
KD3.2
KD3.1
KD1.1
KD2.1
Ctrl1.1
Ctrl1.2
Ctrl2.1
Ctrl3.1
Ctrl2.2
Ctrl3.2
g
Genes representative of the above pathways down-regulated in Ilf2-knockdown
Serpine1
Pmepa1
Fosl2
Bhlhe40
Farp1
Ier3
Errfi1
Nasp
Sdc4
H2ax
Large1
Ext1
Sox4
Sox9
Pdgfb
Cux1
Fn1
Pdgfd
TPM
Ctrl
Ilf2-KD

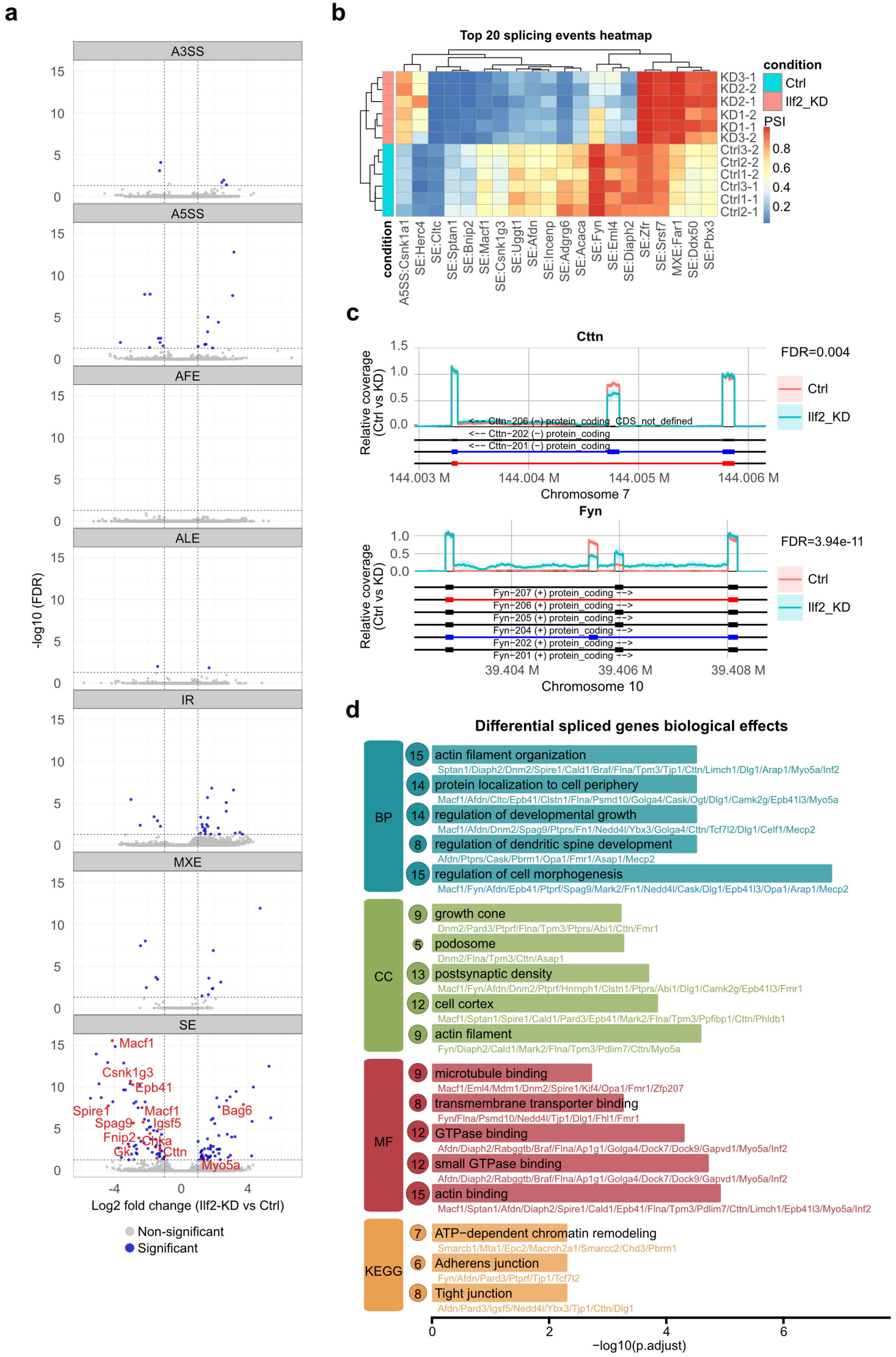
a
A3SS
A5SS
AFE
ALE
IR
MXE
SE
-log10 (FDR)
Macf1
Csnk1g3
Epb41
Spire1
Macf1
Bag6
Spag9
Igsf5
Fnip2
Chka
Gk
Cttn
Myo5a
Log2 fold change (Ilf2-KD vs Ctrl)
Non-significant
Significant
b
Top 20 splicing events heatmap
condition
Ctrl
Ilf2_KD
PSI
KD3-1
KD2-2
KD2-1
KD1-2
KD1-1
KD3-2
Ctrl3-2
Ctrl2-2
Ctrl1-2
Ctrl3-1
Ctrl1-1
Ctrl2-1
condition
A5SS:Csnk1a1
SE:Herc4
SE:Cltc
SE:Sptan1
SE:Bnip2
SE:Macf1
SE:Csnk1g3
SE:Uggt1
SE:Afdn
SE:Incenp
SE:Adgrg6
SE:Acaca
SE:Fyn
SE:Eml4
SE:Diaph2
SE:Zfr
SE:Srsf7
MXE:Far1
SE:Ddx50
SE:Pbx3
c
Cttn
FDR=0.004
Relative coverage (Ctrl vs KD)
Ctrl
Ilf2_KD
<-- Cttn-206 (-) protein_coding_CDS_not_defined
<-- Cttn-202 (-) protein_coding
<-- Cttn-201 (-) protein_coding
144.003 M
144.004 M
144.005 M
144.006 M
Chromosome 7
Fyn
FDR=3.94e-11
Fyn-207 (+) protein_coding -->
Fyn-206 (+) protein_coding -->
Fyn-205 (+) protein_coding -->
Fyn-204 (+) protein_coding -->
Fyn-202 (+) protein_coding -->
Fyn-201 (+) protein_coding -->
39.404 M
39.406 M
39.408 M
Chromosome 10
d
Differential spliced genes biological effects
BP
15 actin filament organization
Sptan1/Diaph2/Dnm2/Spire1/Cald1/Braf/Flna/Tpm3/Tjp1/Cttn/Limch1/Dlg1/Arap1/Myo5a/Inf2
14 protein localization to cell periphery
Macf1/Afdn/Cltc/Epb41/Clstn1/Flna/Psmd10/Golga4/Cask/Ogt/Dlg1/Camk2g/Epb41l3/Myo5a
14 regulation of developmental growth
Macf1/Afdn/Dnm2/Spag9/Ptprs/Fn1/Nedd4l/Ybx3/Golga4/Cttn/Tcf7l2/Dlg1/Celf1/Mecp2
8 regulation of dendritic spine development
Afdn/Ptprs/Cask/Pbrm1/Opa1/Fmr1/Asap1/Mecp2
15 regulation of cell morphogenesis
Macf1/Fyn/Afdn/Epb41/Ptprf/Spag9/Mark2/Fn1/Nedd4l/Cask/Dlg1/Epb41l3/Opa1/Arap1/Mecp2
CC
9 growth cone
Dnm2/Pard3/Ptprf/Flna/Tpm3/Ptprs/Abi1/Cttn/Fmr1
5 podosome
Dnm2/Flna/Tpm3/Cttn/Asap1
13 postsynaptic density
Macf1/Fyn/Afdn/Dnm2/Ptprf/Hnrnph1/Clstn1/Ptprs/Abi1/Dlg1/Camk2g/Epb41l3/Fmr1
12 cell cortex
Macf1/Sptan1/Spire1/Cald1/Pard3/Epb41/Mark2/Flna/Tpm3/Ppfibp1/Cttn/Phldb1
9 actin filament
Fyn/Diaph2/Cald1/Mark2/Flna/Tpm3/Pdlim7/Cttn/Myo5a
MF
9 microtubule binding
Macf1/Eml4/Mdm1/Dnm2/Spire1/Kif4/Opa1/Fmr1/Zfp207
8 transmembrane transporter binding
Fyn/Flna/Psmd10/Nedd4l/Tjp1/Dlg1/Fhl1/Fmr1
12 GTPase binding
Afdn/Diaph2/Rabggtb/Braf/Flna/Ap1g1/Golga4/Dock7/Dock9/Gapvd1/Myo5a/Inf2
12 small GTPase binding
Afdn/Diaph2/Rabggtb/Braf/Flna/Ap1g1/Golga4/Dock7/Dock9/Gapvd1/Myo5a/Inf2
15 actin binding
Macf1/Sptan1/Afdn/Diaph2/Spire1/Cald1/Epb41/Flna/Tpm3/Pdlim7/Cttn/Limch1/Epb41l3/Myo5a/Inf2
KEGG
7 ATP-dependent chromatin remodeling
Smarcb1/Mta1/Epc2/Macroh2a1/Smarcc2/Chd3/Pbrm1
6 Adherens junction
Fyn/Afdn/Pard3/Ptprf/Tjp1/Tcf7l2
8 Tight junction
Afdn/Pard3/Igsf5/Nedd4l/Ybx3/Tjp1/Cttn/Dlg1
−log10(p.adjust)

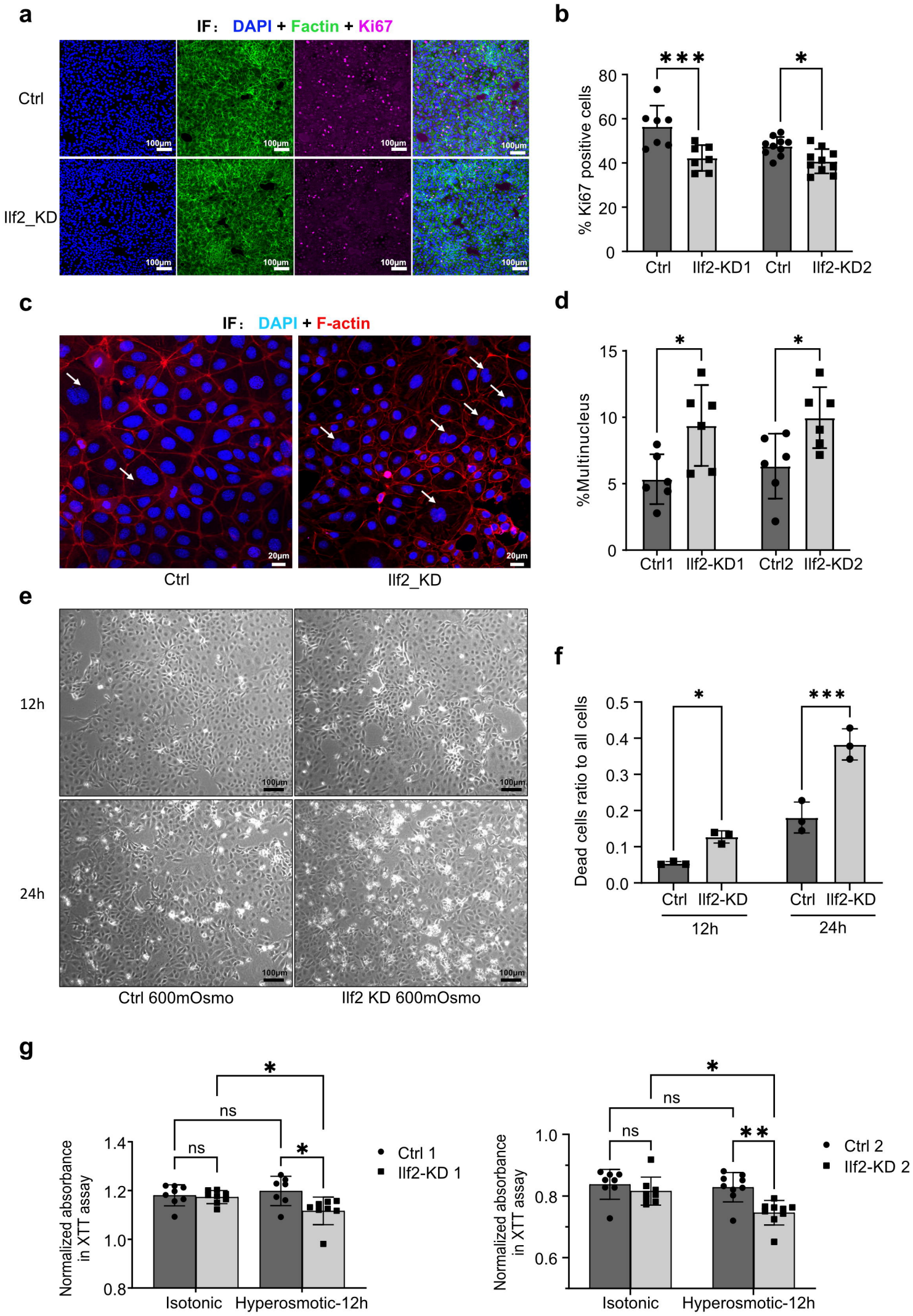
a
IF: DAPI + Factin + Ki67
Ctrl
Ilf2_KD
100μm
b
% Ki67 positive cells
80
60
40
20
0
***
*
Ctrl
Ilf2-KD1
Ctrl
Ilf2-KD2
c
IF: DAPI + F-actin
20μm
Ctrl
Ilf2_KD
d
%Multinucleus
15
10
5
0
*
*
Ctrl1
Ilf2-KD1
Ctrl2
Ilf2-KD2
e
12h
24h
100μm
Ctrl 600mOsmo
Ilf2 KD 600mOsmo
f
Dead cells ratio to all cells
0.5
0.4
0.3
0.2
0.1
0.0
*
***
Ctrl
Ilf2-KD
Ctrl
Ilf2-KD
12h
24h
g
Normalized absorbance in XTT assay
1.4
1.2
1.0
0.8
*
ns
ns
*
Ctrl 1
Ilf2-KD 1
Isotonic
Hyperosmotic-12h
Normalized absorbance in XTT assay
1.0
0.8
0.6
*
ns
ns
**
Ctrl 2
Ilf2-KD 2
Isotonic
Hyperosmotic-12h

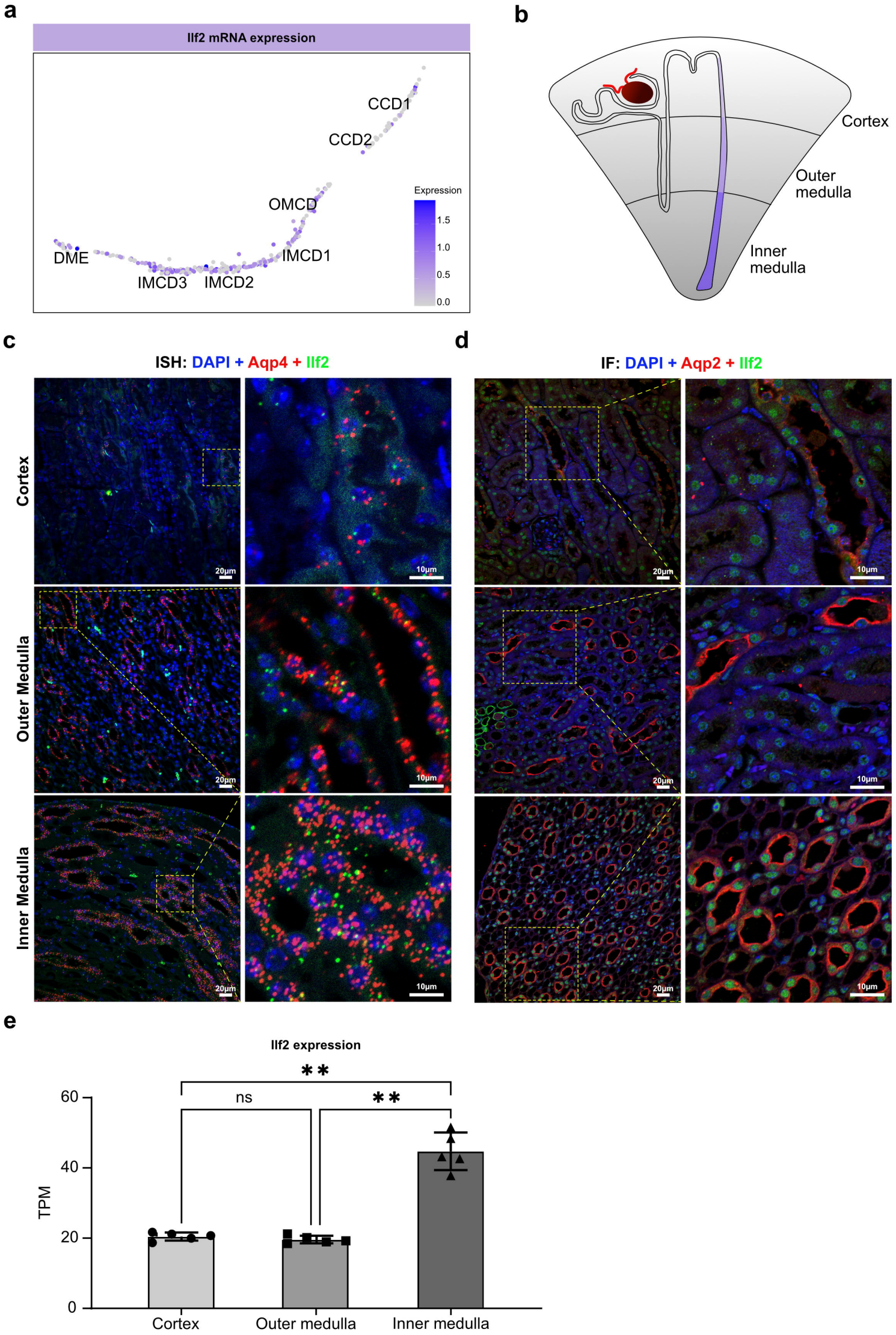
a
Ilf2 mRNA expression
CCD1
CCD2
OMCD
IMCD1
DME
IMCD3
IMCD2
Expression
1.5
1.0
0.5
0.0
b
Cortex
Outer medulla
Inner medulla
c
ISH: DAPI + Aqp4 + Ilf2
Cortex
Outer Medulla
Inner Medulla
20μm
10μm
d
IF: DAPI + Aqp2 + Ilf2
20μm
10μm
e
Ilf2 expression
**
ns
**
60
40
20
0
TPM
Cortex
Outer medulla
Inner medulla

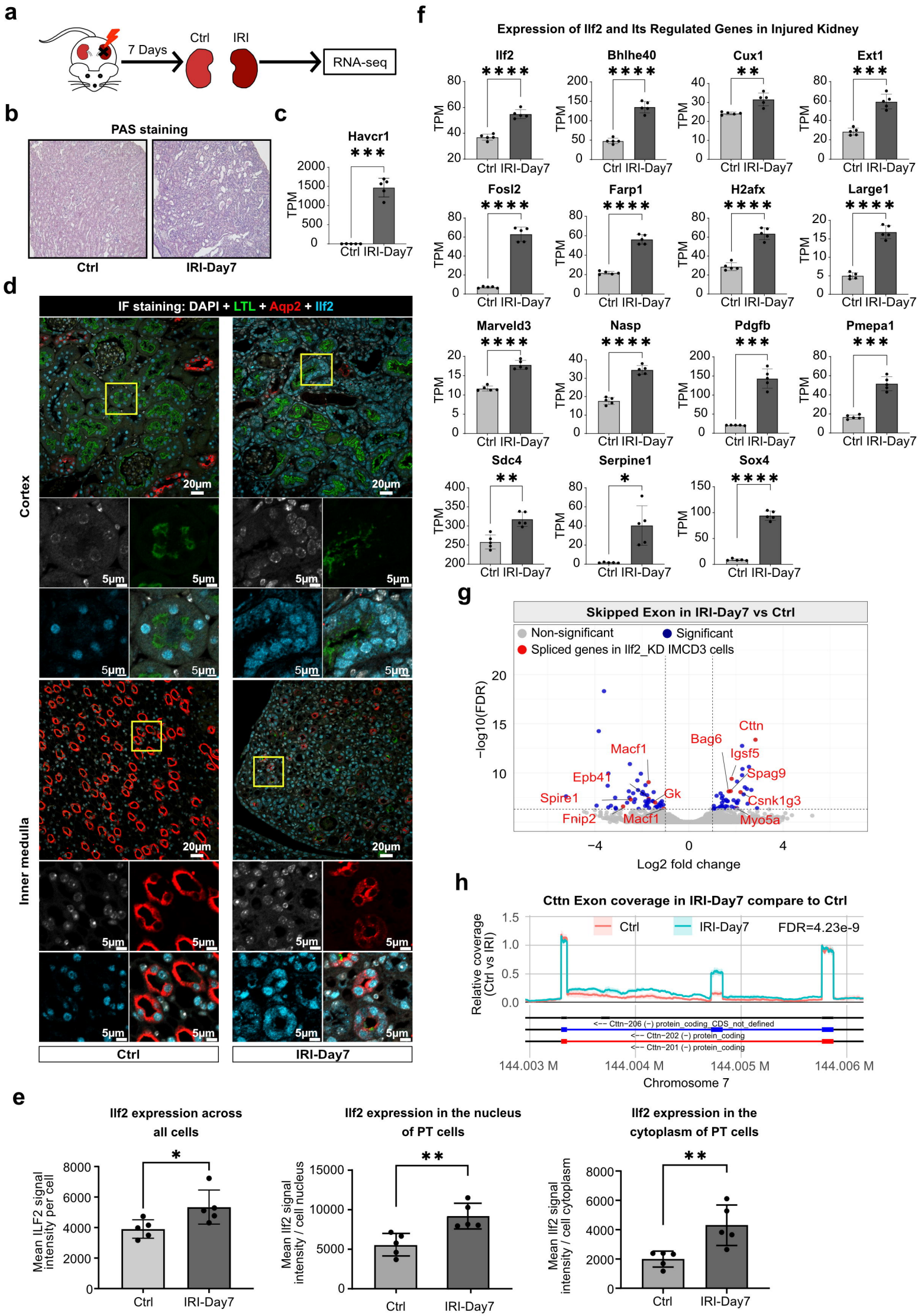
a
7 Days
Ctrl
IRI
RNA-seq
b
PAS staining
Ctrl
IRI-Day7
c
Havcr1
TPM
Ctrl IRI-Day7
d
IF staining: DAPI + LTL + Aqp2 + Ilf2
Cortex
Inner medulla
20μm
5μm
Ctrl
IRI-Day7
f
Expression of Ilf2 and Its Regulated Genes in Injured Kidney
Ilf2
Bhlhe40
Cux1
Ext1
Fosl2
Farp1
H2afx
Large1
Marveld3
Nasp
Pdgfb
Pmepa1
Sdc4
Serpine1
Sox4
TPM
Ctrl IRI-Day7
g
Skipped Exon in IRI-Day7 vs Ctrl
Non-significant
Significant
Spliced genes in Ilf2_KD IMCD3 cells
−log10(FDR)
Log2 fold change
Cttn
Bag6
Igsf5
Spag9
Csnk1g3
Myo5a
Macf1
Epb41
Spire1
Fnip2
Gk
h
Cttn Exon coverage in IRI-Day7 compare to Ctrl
Ctrl
IRI-Day7
FDR=4.23e-9
Relative coverage (Ctrl vs IRI)
<-- Cttn-206 (-) protein_coding_CDS_not_defined
<-- Cttn-202 (-) protein_coding
<-- Cttn-201 (-) protein_coding
144.003 M
144.004 M
144.005 M
144.006 M
Chromosome 7
e
Ilf2 expression across all cells
Mean ILF2 signal intensity per cell
Ilf2 expression in the nucleus of PT cells
Mean Ilf2 signal intensity / cell nucleus
Ilf2 expression in the cytoplasm of PT cells
Mean Ilf2 signal intensity / cell cytoplasm
Ctrl
IRI-Day7